nature protocols

PROTOCOL

https://doi.org/10.1038/s41596-019-0201-3

Quantum diamond spectrometer for nanoscale NMR and ESR spectroscopy

Dominik B. Bucher[1,2*], Diana P. L. Aude Craik[2], Mikael P. Backlund[1,2], Matthew J. Turner[2], Oren Ben Dor[1,2], David R. Glenn[2] and Ronald L. Walsworth[1,2*]

Nitrogen-vacancy (NV) quantum defects in diamond are sensitive detectors of magnetic fields. Owing to their atomic size and optical readout capability, they have been used for magnetic resonance spectroscopy of nanoscale samples on diamond surfaces. Here, we present a protocol for fabricating NV diamond chips and for constructing and operating a simple, low-cost 'quantum diamond spectrometer' for performing NMR and electron spin resonance (ESR) spectroscopy in nanoscale volumes. The instrument is based on a commercially available diamond chip, into which an NV ensemble is ion-implanted at a depth of ~10 nm below the diamond surface. The spectrometer operates at low magnetic fields (~300 G) and requires standard optical and microwave (MW) components for NV spin preparation, manipulation, and readout. We demonstrate the utility of this device for nanoscale proton and fluorine NMR spectroscopy, as well as for the detection of transition metals via relaxometry. We estimate that the full protocol requires 2–3 months to implement, depending on the availability of equipment, diamond substrates, and user experience.

Introduction

Magnetic resonance spectroscopy of electrons and nuclei comprises a family of ubiquitous and essential analytical tools in modern chemical and biological research[1]. ESR—also known as electron paramagnetic resonance (EPR)—spectroscopy is a useful means for probing molecules possessing unpaired electrons, such as transition-metal complexes and radicals[2]. (Bio)molecules that lack an unpaired electronic spin can be probed via ESR-active spin labels. NMR, on the other hand, is a more widely used technique, as NMR-active nuclei (e.g., ^{1}H, ^{13}C, ^{14}N, and ^{31}P) are commonly encountered in organic and biological chemistry. The narrow spectral lines of NMR afford unprecedented information about molecular structure and dynamics. NMR is less sensitive than ESR, however, owing to the lower gyromagnetic ratios of nuclei compared to that of the electron. In fact, both NMR and ESR are relatively insensitive as compared to the state of the art in other analytical techniques, such as mass spectrometry and fluorescence microscopy. The low sensitivity of magnetic resonance is particularly challenging for life science applications, in which biomolecules of interest commonly occur in small absolute quantities or concentrations. Thus, there is great interest in new techniques to increase the sensitivity of magnetic resonance spectroscopy[3–5]. One promising approach uses a magnetic sensor based on fluorescent quantum defects in diamond, such as NV color centers, enabling interrogation of sample volumes down to the nanoscale[6,7], including single proteins[8,9], single protons[10], and 2D materials[11]. In this protocol, we describe the procedure for generating NV-diamond sensor chips and the construction of a quantum diamond spectrometer for NMR and ESR of nanoscale samples placed on the diamond chip.

Physical background

NV diamond quantum sensor

NV color centers are atomic-scale quantum defects that provide high-resolution magnetic field sensing and imaging via optically detected magnetic resonance (ODMR), with broad applicability in both the physical and life sciences. NVs have been reviewed extensively elsewhere[12–16]; and so we give only a brief overview here to introduce the concepts that are most important to the present work. An NV center is created when two neighboring carbon atoms in the diamond lattice are replaced by a nitrogen atom and a vacancy (Fig. 1b), resulting in local C_{3v} symmetry. The point-like defect has

[1]Harvard-Smithsonian Center for Astrophysics, Cambridge, MA, USA. [2]Department of Physics, Harvard University, Cambridge, MA, USA.
*e-mail: dominik.bucher@tum.de; rwalsworth@cfa.harvard.edu

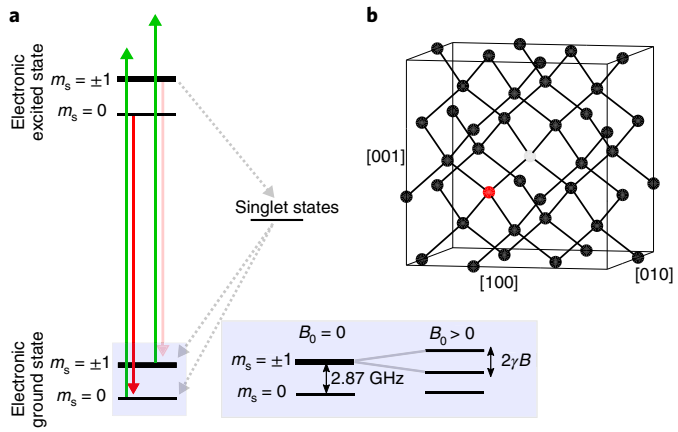

Fig. 1 | NV center overview. a, Simplified energy-level diagram of an NV center. A 532-nm laser (green arrows) can be used to optically excite an NV from the spin-triplet ground state to the spin-triplet excited state. From the excited-state manifold, the NV can emit a red-shifted photon (red arrows) by photoluminescence (PL). The $m_s = \pm 1$ states are dimmer than the $m_s = 0$ state because of a competing nonradiative decay (gray dotted arrows) that causes NVs to reach spin-singlet states that lie between the two spin-triplet states in regard to energy. For sensing applications, one typically drives transitions between two spin sublevels (e.g., $m_s = 0$ to $m_s = +1$ or $m_s = -1$) of the electronic ground state (inset). **b**, Sketch of an NV center and surrounding diamond lattice. An NV is formed by substituting two neighboring carbon atoms (black circles) with a nitrogen atom (red) and a vacancy (light gray). Miller indices [hkl] indicate lattice vectors in the direction of the labeled edges.

electronic states that sit within the band gap of diamond, a fact that allows one to address the energy levels of the NV in a manner analogous to the manipulation of molecular or atomic levels. The NV center can exist in several charge states, of which the most widely studied is the negatively charged NV−, with electronic spin $S = 1$ in its ground state. Throughout this protocol, we use the term 'NV center' synonymously with 'NV−'. A zero-phonon splitting of 637 nm separates the electronic spin-triplet ground and excited states. Each of these states is further split by higher-order interactions, some of which are described below. A broad phonon side band allows one to prepare and read out the NV spin state with absorption of blue-shifted light (e.g., from a 532-nm laser) and then detection of the red-shifted photoluminescence (PL) (Fig. 1a).

NV centers have drawn considerable interest in recent years as a tool for sensing, especially sensing of magnetic fields[13,15,17]. For these applications, the splittings of the eigenstates of the z-component of the electron spin operator S_z are of particular importance, where z refers to the axis connecting the nitrogen atom and vacancy (i.e., the line connecting the red and light gray dots in Fig. 1b). Such splittings in the electronic ground state can be understood by considering the relevant (simplified) spin Hamiltonian:

$$\mathcal{H} = DS_z^2 - \gamma_e \mathbf{B} \cdot \mathbf{S}, \quad (1)$$

where $D = 2.87$ GHz, $\mathbf{S} = (S_x, S_y, S_z)^T$ is the electronic spin operator, $\gamma_e = 2.8$ MHz/G is the electron's gyromagnetic ratio[14], and $\mathbf{B}$ is an external magnetic field that in this work consists of a strong applied field along z (B_0) plus a weak 'signal field' to be sensed $\left(B_z^{(\text{sense})}\right)$. The first term on the right-hand side of Eq. 1 describes a zero-field splitting due to spin–spin interactions[17]. The second term describes the Zeeman interaction with the magnetic field. For a sufficiently weak signal field, the NV is largely sensitive to the z component such that:

$$\mathcal{H} = DS_z^2 - \gamma_e\left(B_0 + B_z^{(\text{sense})}\right)S_z. \quad (2)$$

Thus, the signal field has the effect of shifting the spin state $m_s = \pm 1$ by $\pm\gamma_e B_z^{(\text{sense})}$ (Fig. 1a, inset). Transitions between ground electronic states of different m_s values are driven by application of a resonant MW field. A sensing sequence consists of a specified set of MW pulses followed by readout of the final spin state. Spin-state readout is enabled by the fact that NVs emit fewer PL photons on average when optically excited from $m_s = \pm 1$ than they do from $m_s = 0$, owing to a substantial probability of decaying via an alternative pathway mediated by singlet electronic states in the former case (Fig. 1a). Thus, an NV ensemble with more population in $m_s = \pm 1$ fluoresces less brightly than one with more population in $m_s = 0$.

The other important characteristic that enables optically detected magnetic sensing with NVs is the ability to initialize the spin state. At thermal equilibrium, each of the three m_s sublevels in the electronic ground state is roughly equally populated. However, a laser pulse of sufficient duration results in nearly complete polarization into the $m_s = 0$ state, a consequence of the unequal non-radiative decay rates[18]. Thus, an arbitrary (nearly) pure state can be obtained at the onset of a measurement by application of an initializing laser pulse followed by the appropriate MW pulse. This initialization step is a common motif in the nuclear and electronic spin sensing protocols presented herein.

NV-mediated sensing can be implemented with either a single NV or an NV ensemble. On the one hand, single-NV sensing allows for atomic-scale spatial resolution. On the other hand, ensemble averaging leads to a sensitivity improvement roughly proportional to the reciprocal square root of the number of sensor NVs.

Nuclear spin sensing

When exposed to a static magnetic field of a few hundred gauss, nuclear spins generate NMR signals, i.e., oscillating (denoted as AC) magnetic fields (B_{AC}), with frequencies between hundreds of kilohertz and a few megahertz. In the protocol presented here, these NMR fields are sensed with a near-surface NV ensemble layer. Importantly, each NV is primarily sensitive to NMR fields generated by nuclear spins within a hemisphere volume above the diamond, with the radius set by the depth of the NV beneath the surface[6,19–21]. For instance, NVs that have been implanted 10 nm beneath the diamond surface sense NMR signals from a surface layer of ~10 nm thickness. In such nanoscale volumes, the number of spins is relatively small, and so the statistical polarization $\left(\sim 1/\sqrt{\text{number of spins}}\right)$ exceeds the thermal spin polarization (~10^{-7}–10^{-5} for 0.1- to 10-T fields at room temperature (°C))[22]. An appropriate AC magnetometry pulse sequence can be used to measure the fluctuations of the statistical polarization[23,24]. As mentioned above, all pulse sequences start with a short laser pulse to initialize the NV into the $m_s = 0$ ground sub-state. Each sequence ends with a laser pulse to read out the quantum state via detection of the PL (Fig. 2a). Between these two laser pulses, MW pulse sequences are applied to manipulate the NV quantum state in accordance with a chosen sensing protocol. The AC magnetometry pulse sequence begins with a $\pi/2$ pulse, which generates a quantum coherence between the $m_s = 0$ and $m_s = -1$ states by rotating the Bloch vector corresponding to the NV quantum state to the equator of the Bloch sphere (Fig. 2b). This coherent superposition is then allowed to evolve for a specified free precession time, during which it accumulates phase in a manner that depends on the magnetic field being sensed. A final $\pi/2$ pulse maps the accumulated phase into a population difference between $m_s = 0$ and $m_s = -1$, which is translated into a change in the NV fluorescence rate during the laser readout pulse. During free precession, a train of π pulses with defined phases, termed a dynamic decoupling sequence (for instance, an XY8-N sequence, described in refs. [25,26]), is applied. The purpose of this sequence is twofold: it extends the NV coherence time and creates a narrowband detector for magnetic signals with frequency near $f = 1/(2\tau)$, where τ is the spacing between pulses. In the case of an XY8-N sequence, the block of eight π pulses is repeated N times, where choice of N depends on τ and the decoherence properties of the NVs. In subsequent measurements, τ is typically swept. When the condition

$$\tau = \frac{1}{2f_0}, \tag{3}$$

is satisfied, where f_0 is the Larmor frequency of the sample spins, the NV center accumulates maximum phase, leading to a measurable reduction in the NV fluorescence rate during the readout laser pulse. The XY8-N pulse sequence has been usefully applied in sensing surface nuclear spins[6,8,20].

However, experiments have shown that this pulse sequence can also pick up signals from higher harmonics of f_0, which can lead to ambiguous results[27]. This issue can be overcome by correlating two consecutive sensing pulse sequences[24,28–30]. This so-called 'correlation spectroscopy' consists of two XY8-N sequences, separated in time by t_{corr}, which is swept during the experiment (Fig. 2c). The NV-phase accumulation in a dynamic decoupling sequence depends on the relative phase ϕ of the sensed magnetic AC field. Intuitively, if t_{corr} is an integer multiple of $1/f_0$, both XY8-N sequences accumulate the same NV phase (as ϕ is identical) and the correlation signal is at its maximum. If t_{corr} is a half-integer multiple of $1/f_0$, the readout signal is at its minimum, because the magnetic AC field phase ϕ is out of phase. As t_{corr} is swept, the resulting PL readout signal oscillates at the nuclear spin Larmor frequency in a manner similar to the free induction decay in conventional NMR.

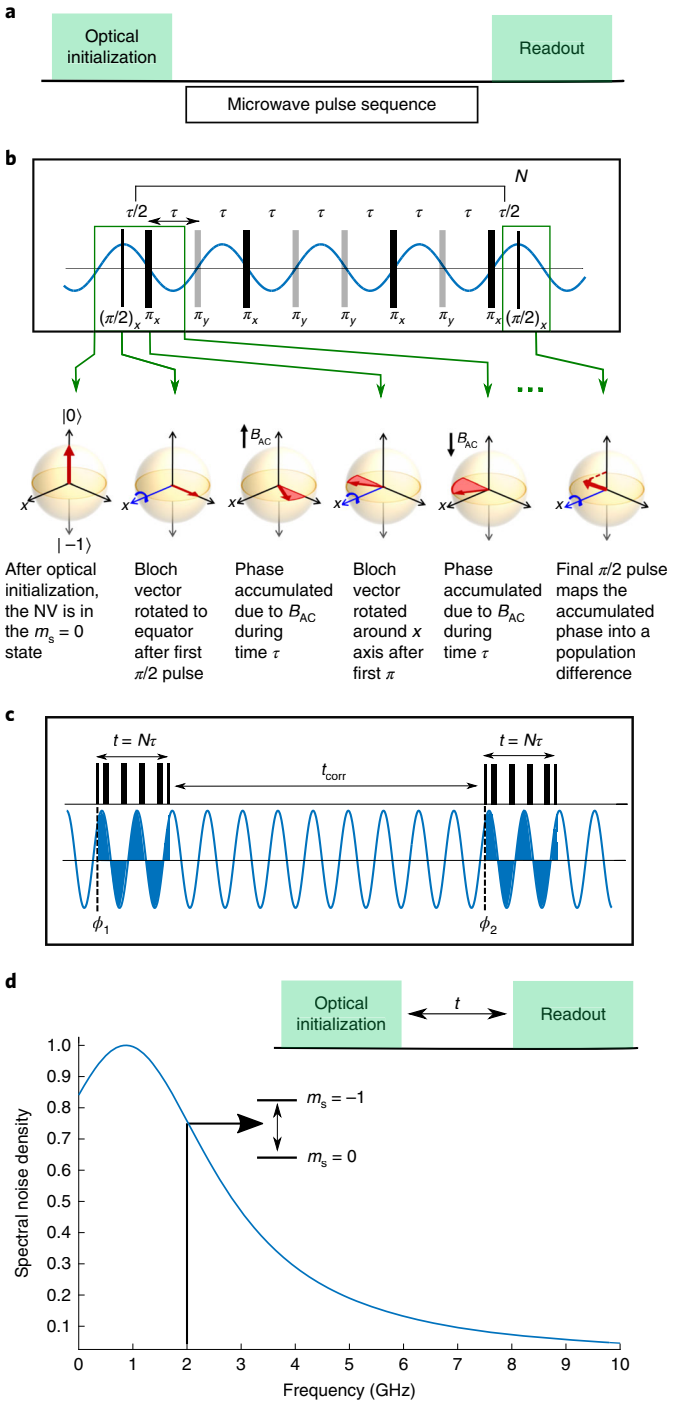

Fig. 2 | Nuclear and electronic spin-sensing schemes with NV centers. a, All pulse sequences start with an optical initialization pulse, followed by a microwave pulse sequence for NV-spin control and sensing, and then end with an optical pulse for fluorescence readout. **b**, An XY8-*N* dynamic decoupling pulse sequence is used as a sensing scheme for AC magnetic fields. The NV accumulates phase if half of the AC period coincides with the spacing τ of the π pulses. This accumulated phase can be detected as a dip in the NV-T2 relaxation curve. The rotation axes of the XY8-*N* pulses are indicated as subscripts, i.e., π_x and π_y. Bottom, the corresponding Bloch sphere diagrams are shown. **c**, The correlation spectroscopy pulse sequence consists of two XY8-*N* sequences with fixed τ at half of the AC field period. The timing t_{corr} is swept, which correlates the phases ϕ of the AC magnetic field and generates oscillations in the readout data at the AC frequency. **d**, External nuclear spins (e.g., Cu^{2+} or Gd^{3+}) are sensed by the spectral noise around the NV transition frequency (shown here at 2 GHz, corresponding to an applied field of ~300 G), which leads to an increase in NV-T1 relaxation. The width of the spectral noise density δ depends on the rate of electronic spin flips (shown here for $\delta = 2$ GHz). Inset shows a typical pulse sequence for measuring the NV-T1 relaxation time, consisting of optical initialization and readout pulses separated by time *t*, where *t* is varied over of the experiment.

The NV center has been successfully used to detect NMR signals from nanoscale sample volumes[6,20,30], single proteins[8], single protons[10], and 2D materials[11]. Many of these experiments have been performed with a single NV sensor, but one can also take advantage of an ensemble of NV sensors for both wide-field imaging[20] and enhanced sensitivity[31].

Limitations of nuclear spin sensing with NV centers

High-frequency resolution (of a few Hertz) is important for resolving molecular structures via chemical shifts and scalar (i.e., 'J') couplings. The nanoscale NV experiments described above are limited in that they provide only modest frequency resolution (typically of 1–100 kHz). This limitation is due to two reasons: (i) measured linewidths are limited by NV-T2 relaxation when sensing is performed using dynamical decoupling sequences and by NV-T1 relaxation when correlation spectroscopy is used. As NV-T2 < NV-T1, correlation spectroscopy gives superior frequency resolution, as good as ~100 Hz. (ii) Unfortunately, this frequency resolution is usually not achieved in nanoscale NV-NMR experiments. Sample diffusion limits the interaction time between the NV sensor and the nuclear spin, resulting in short correlation times τ_c and broadened lines. The linewidth (LW) depends on the diffusion coefficient (D) and the NV depth (d), as described in the following equation:

$$\mathrm{LW} \approx \frac{1}{\pi\tau_c} = \frac{6D}{\pi d^2} \tag{4}$$

For instance, for a 10-nm-deep NV, signals produced by protons in water give rise to linewidths of ~40 MHz and viscous oil signals produce linewidths of ~10 kHz.

Recent experiments have overcome some of these limitations through two approaches. The first approach uses nuclear spins in the diamond as a quantum memory to extend the readout time, enabling resolution of chemical shifts at high magnetic fields (~3 T)[32]. In this approach, statistical polarization is detected from nanoscale sample volumes, and linewidths remain limited by sample diffusion. Our group recently demonstrated an alternative 'synchronized readout' approach based on XY8-N sequences that achieved linewidths on the order of 1 Hz and thereby enabled chemical shift and J-coupling resolution[33,34]. In these experiments, we overcome the diffusional line broadening by detecting thermal spin polarization in an ~$(10\text{-}\mu\mathrm{m})^3$ volume. These new developments are not described in further detail in this protocol, as they require advanced technical expertise and equipment. The more basic NV-NMR methods described here are useful for detecting NMR signals from nanoscale surface layers. Practical applications are structural analysis of quadrupolar nuclei in 2D materials[11], NMR microscopy[20], and molecular dynamics at interfaces[30].

Compared to conventional liquid-state NMR with an inductive detection scheme, the NV diamond sensor has two main advantages: (i) the detection of very small sample volumes—down to a single molecule or nanometer surface layers (described in this protocol), and (ii) the potential to perform NMR microscopy and nanoscopy, enabled by the optical nature of NV readout. On the other hand, for some applications, the reduction of the sample volume associated with NV-NMR relative to conventional NMR can pose a disadvantage, e.g., because of the diffusive broadening mentioned above.

Electronic spin sensing

Electronic spins resonate at much higher frequencies (~600×) than nuclear spins at the same magnetic field. Such high frequencies (~1 GHz for a magnetic field of a few hundred gauss) cannot be detected with NVs using dynamic decoupling sequences because of the finite duration of the MW pulses (a few tens of nanoseconds). Here, an alternative detection protocol, NV relaxometry, is used[13,35,36]. Magnetic noise generated by electronic spins is caused by spin flips, with a timescale set by their T1 relaxation time. The noise can be described by its spectral density $S(f) \sim \delta/((f-f_L)^2+\delta^2)$, where f_L is the electronic spin Larmor frequency. The spectral density is broadened by the spectral width δ, which is the inverse of the T1 relaxation time of the electronic spin (Fig. 2d). δ is typically on the order of a few hundreds of megahertz for Cu^{2+} (Simpson et al.[37]) to 10 GHz for Gd^{3+} (Sushkov et al.[36]). Thus, $S(f)$ usually features significant noise components around the NV transition frequency (~2 GHz), which lead to a reduction of the NV-T1 relaxation rate $\Gamma_{total} = \Gamma_{intr} + \Gamma_{induced}$, where Γ_{total}, Γ_{intr} and $\Gamma_{induced}$ are the measured relaxation rate, the intrinsic relaxation rate (in the absence of noise) and the induced relaxation rate due to noise, respectively. In a typical experiment, the NV-T1 relaxation time is measured by optically initializing the NV into the $m_s = 0$ ground state and allowing its quantum state to thermalize for a time t according to Γ_{total}. The NV spin state is read out via an optical pulse as a function of t and the decay of the polarization can be fitted to an exponential

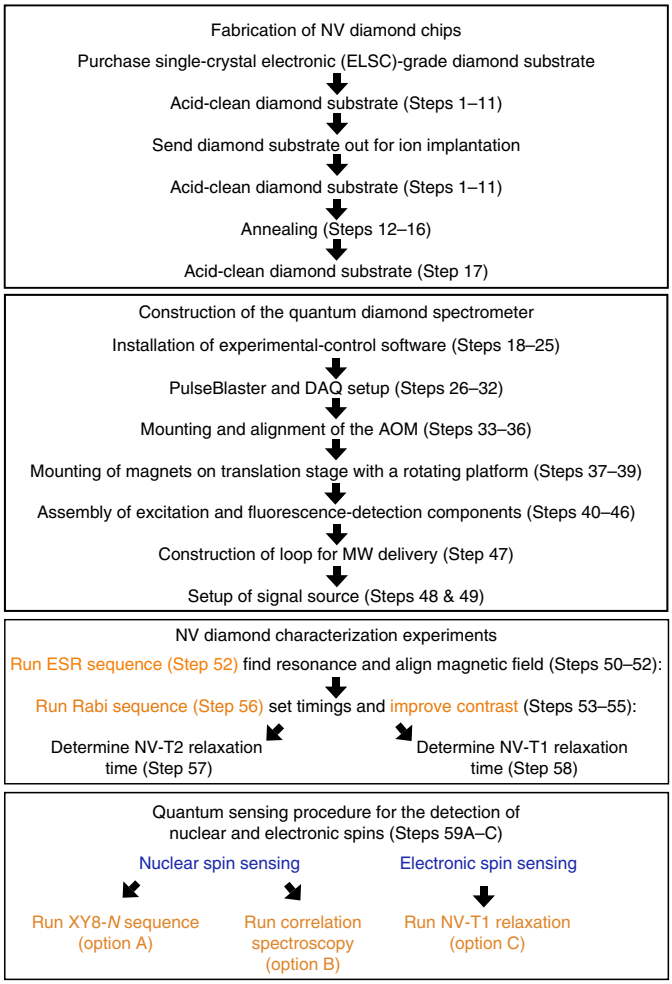

Fig. 3 | Overview of the procedure. The procedure is divided into four parts: (i) fabrication of the NV diamond chip (Steps 1–17), (ii) construction of the quantum diamond spectrometer (Steps 18–49), (iii) NV diamond characterization experiments (Steps 50–58), and (iv) a quantum sensing procedure for sensing nuclear and electronic spins (Step 59A–C). Steps for daily use are marked in orange.

function. Possible applications for nanoscale electronic spin sensing include the detection of biologically important ions[35,37] or metalloproteins[38] in cells.

Limitations of electronic spin sensing with NVs

NVs are initialized and read out with green laser pulses. Although the light intensity reaching the sample is reduced by the total internal reflection geometry used in this protocol, the evanescent wave at the sample's surface may be sufficient to excite the sample. This may cause problems when samples that absorb green light are measured (e.g., various colored transition-metal complexes), possibly inducing unwanted photochemistry and sample degradation[39].

Overview of the procedure

First, we discuss the experimental design and the required hardware. Second, we describe the technical details of the specific pulse sequences used for sensing. Finally, we describe the experimental procedure itself, which in turn is organized into four parts (Fig. 3): (i) the fabrication of NV diamond chips to be used as sensors (Steps 1–17), (ii) the construction of the quantum diamond spectrometer (Steps 18–49), (iii) NV diamond characterization experiments (Steps 50–58), and (iv) quantum sensing procedure for sensing nuclear and electronic spins (Step 59). The last two parts describe the procedure to run all basic pulse sequences and the procedure to detect NMR and EPR signals on the nanoscale.

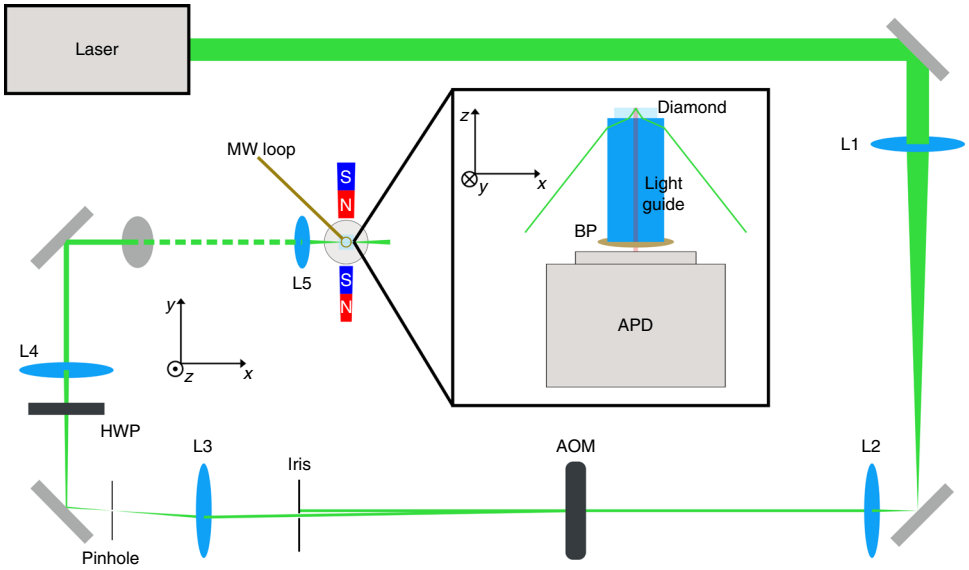

Fig. 4 | Schematic of optical components. The 532-nm laser beam is passed through a telescope consisting of lenses L1 ($f = 400$ mm) and L2 ($f = 50$ mm) in order to demagnify the beam waist by a factor of 8. The small collimated beam is then passed through the acousto-optic modulator (AOM). An iris placed after the AOM blocks the zeroth diffraction order and passes the first diffraction order. Additional optical extinction is achieved by focusing the beam through a 200-µm pinhole with lens L3 ($f = 100$ mm). A $\lambda/2$ waveplate (HWP) is used to rotate the polarization in order to maximize contrast in the NV measurement. The lens L4 ($f = 200$ mm) again collimates the beam. The last mirror in the setup is oriented such that the beam is sent out of the *xy* plane, now with its Poynting vector parallel to the *xz* plane (indicated by the dashed green line). A short-focal-length lens L5 ($f = 30$ mm) focuses the beam into the NV layer within the diamond under a total internal reflection geometry. Here we show an example for a diamond chip with unpolished edges such that the light must be coupled in through a light guide. At this point in the setup, an MW loop and a pair of permanent magnets (with S and N denoting magnetic south and north poles, respectively) are positioned. The perspective on the bar magnet illustration is meant to convey that it is oriented at an angle of ~36° relative to the *xy* plane. Inset: rotated view down the *y* axis of the excitation and detection. The laser is passed through the side of the light guide at an angle such that light is efficiently transmitted from glass into the diamond and then exhibits total internal reflection at the diamond–air interface. PL is collected through the light guide and passed through a band-pass fluorescence filter (BP) before being detected by the avalanche photodiode (APD).

Experimental design

In the following, we discuss the technical design choices made and equipment used in the development and implementation of this protocol. Figures 4 and 5 give overviews of the optics and electronics, respectively, that are used in this protocol.

Choice of diamond substrate and nitrogen implantation

Ultra-pure diamonds with low concentration of defects (nitrogen concentration <10 p.p.b.) are needed to maximize the probability of creation of NV centers with long coherence times and optimized sensing properties. Traditionally 'electronic-grade single-crystal' diamonds from Element Six (https://e6cvd.com/us/application/all.html) have been used as substrates. Another potential source of diamond substrates is LakeDiamond (https://lakediamond.ch/products), which offers 'ultra pure diamond plates'. Depending on the user's application, a ^{12}C-enriched substrate might be necessary to decrease the NMR signal from natural-abundance ^{13}C. The choices of diamond size and shape depend on the requirements of the experiment and may be limited by the availability of large substrates. Our diamond is cut such that the top face is perpendicular to the [100] crystal axis, and the lateral faces are perpendicular to [110]. Ideally, the edges of the diamond are polished so that the NV layer can be excited through the edge in a total internal reflection geometry. Nanostructured diamond surfaces have been shown to increase magnetic resonance sensitivities[31]. Shallow NV centers are needed for surface sensing and are typically created through bombardment of the diamond sample with low-energy nitrogen ions. To produce shallow NVs at depths of a few nanometers, the implant energy is typically between 2.5 and 6 keV[21,40]. Such shallow NVs exhibit degraded spin properties[41–43], although NMR signals from samples on the diamond surface are larger because of the proximity of the NVs to the sample. Monte Carlo simulations (stopping and range of ions in matter (SRIM))[44] can be performed to calculate the

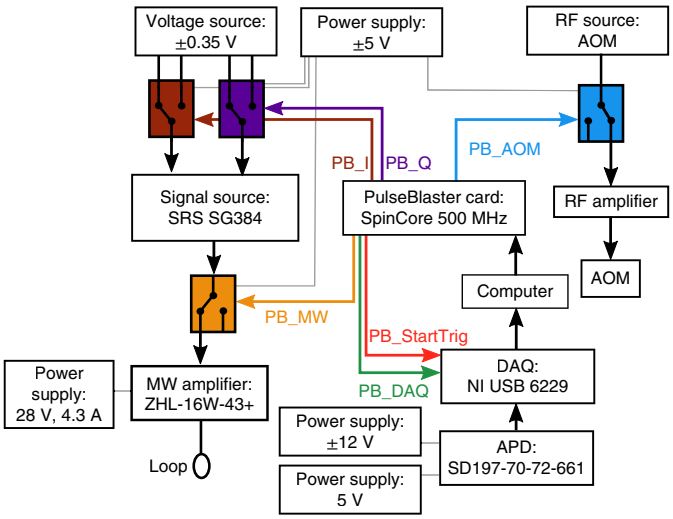

Fig. 5 | Schematic of electronic components. Colors indicate the six PulseBlaster TTL signal outputs used in the pulse sequences outlined in Fig. 6. Arrows indicate the direction of information flow.

approximate depth of the created defect as a function of nitrogen ion implantation energy and angle of incidence. An implant angle of ~5–7° from the normal is usually chosen to minimize channeling (i.e., to keep the implanted ions shallow). If one implants ions exactly normal to the surface, then the implanted ions can better channel through the crystal lattice and penetrate deeper into the crystal than one would naively expect from calculations[45]. An estimate of the NV depth can be obtained from NV-NMR experiments as described for single NV centers in Pham et al.[21].

For AC magnetometry, nitrogen ion implantation is usually done with ^{14}N ($I = 1$), which has a hyperfine structure that does not greatly interfere with NV sensing. By contrast, ^{15}N ($I = 1/2$) tends to give background that is sensitive to misalignment of the bias field B_0.

Following implantation, the diamonds are annealed under vacuum (typically $<10^{-6}$ mbar; $<2 \times 10^{-8}$ mbar in this instance) and high temperature (800–1,200 °C) to allow migration of vacancies and formation of NV centers. High-temperature processing also allows one to minimize interactions with neighboring spins by annealing out other spin impurities. There are limitations to how much annealing can improve the spin bath properties and formation of NVs; this is still an active area of research, especially for high-density shallow-implantation diamonds[40,46,47]. We anneal diamonds in an in-house-built furnace. However, owing to the complexity of setting up an annealing system, we suggest either sending out the diamond sample to another research group with a working furnace or using a commercial option (e.g., http://www.laserage.com/heat-treating). Following annealing of the sample, one can observe and measure several different characteristics of the sample to characterize success or failure of the annealing. Upon annealing, a gray tint to the color of the diamond indicates the presence of surface graphitization. Acid cleaning is needed to remove this graphitized layer. For some applications, AFM may be needed to check the roughness of the diamond if surface damage is important to the specific application. One can characterize the fluorescence intensity (counts) and the coherence time (NV-T2) of the NVs before and after the annealing to characterize the creation of NVs or the presence of unwanted defects.

The efficiency of NV creation depends on both the ion energy and the ion fluence[48], which should be chosen such that, for high-density, shallow layers, the nitrogen atom areal density is in the range 10^{12}–10^{14} cm^{-2}, ultimately producing an NV areal density in the range of 10^{11}–10^{12} cm^{-2}. Given that the expected NV density is below the measurement threshold for traditional bulk measurement techniques such as UV-visible, Fourier-transform infrared spectroscopy (FTIR), or EPR, one must perform confocal measurements to characterize the counts. For ultra-low-density samples, in which single NVs are spatially resolvable, one can perform a spatial survey of NVs and count individual centers to calculate the density. For the types of samples used in this paper, in which single NVs are not resolvable, one must use the average count rate in a confocal volume to determine the density. Using a rough reference value of a typical single NV count of ~50–100 kcounts/s (around optical saturation), one can obtain an approximate value for the number of NVs in a volume by normalizing to the single NV reference counts.

Moreover, work to understand the surface and mitigate surface noise is an active area of research and there exist other protocols to improve coherence times and fidelity of near-surface NV centers[8,40,41,43,49–52]. We present in this protocol one method for fabrication and preparation that is relatively accessible and robust in its results. More sensitive applications than the ones demonstrated in this work will require better control of the surface and the implementation of various other methods cited above.

The diamond chip described in this work is an E6 CVD 99.6% ^{12}C layer (50–100 μm) on a natural-abundance substrate. Nitrogen (^{14}N) implantation was carried out by sending the diamond to a commercial e-beam facility (INNOViON), where it was implanted with a nitrogen ion beam of energy (6 keV) and a fluence of 2×10^{13} cm^{-2}. We estimate the final NV density for this diamond to be $\approx 3 \times 10^{11}$ cm^{-2}.

Surface contamination of the diamond substrate can be removed through the use of a 1:1:1 refluxing mixture of sulfuric, nitric, and perchloric acid. This solution should be used to clean the diamond before implantation to ensure surface contaminants are not present. Cleaning should be repeated before and after annealing to remove any graphitization buildup on the diamond surface. This cleaning procedure is also applied to remove and mitigate any undesirable effects observed during sensing protocols; these can occur because of surface contamination[53,54].

Choice of magnets

Permanent magnets are generally preferred to electromagnets for reasons of simplicity and cost, and because of stringent requirements on the stability of the current sources used to power the latter. In principle, any commercial permanent magnets can be used, as long as they generate a field B_0 of at least a few hundred gauss at a distance of a few centimeters from their surface. The field strength B_0 is important for nuclear spin sensing because it defines the Larmor frequency f_L according to

$$f_L = \gamma_n B_0, \tag{5}$$

where γ_n is the gyromagnetic ratio of the spin of interest and B_0 is the field strength at the sample position. Gyromagnetic ratios for different nuclei are provided, e.g., by the Committee on Data of the International Council for Science (www.codata.org). For efficient NV detection with a dynamic decoupling sequence, the Larmor frequencies of the target nuclear spins should be between a few hundred kilohertz and a few megahertz. Magnets can be stacked to increase magnetic field strength.

In all cases, magnetic field gradients should be kept as small as possible in order to suppress inhomogeneous broadening. The use of two identical magnets, with poles aligned, placed on opposite sides of the sample, and having diameter at least on the order of a few centimeters (i.e., much larger than the laser spot size of ~20 μm) helps to minimize field gradients. For a detailed analysis of the magnetic field distribution of a given permanent magnet geometry, the software package Radia (http://www.esrf.eu/Accelerators/Groups/InsertionDevices/Software/Radia) in Mathematica (http://www.wolfram.com/mathematica/) can be used. A common issue with static magnets is their temperature-dependent magnetization. To mitigate this problem, we use samarium–cobalt magnets, which have a low temperature dependence (0.001%/°C).

Choice of laser source and acousto-optic modulator

To excite the NV ensemble, a 532-nm laser with ~1-W output power is used. We recommend using a high-quality optically pumped semiconductor laser (OPSL) or a diode-pumped solid-state (DPSS) laser (e.g., Coherent Verdi G series or Lighthouse Photonics Sprout series of lasers). However, lower-priced 1-W laser diodes can also be used, at the expense of inferior noise properties.

For the sensing protocol described here, laser pulses on the microsecond timescale are necessary for initializing and reading out the NVs. We recommend using an acousto-optic modulator (AOM) with a drive frequency of ≥80 MHz or higher (e.g., IntraAction ATM-801A2) to achieve high extinction ratios. The AOM can be driven either by a commercially available AOM driver (which will include a signal source and amplifier) or by a radio frequency (RF) signal source operating at the specified AOM drive frequency and amplified to reach the required RF power level. We use a commercial AOM driver (IntraAction ME-802N), which is usually modulated by a voltage input. However, we achieved better performance (i.e., a larger extinction ratio) by inserting a switch between its internal signal source and amplifier.

Choice of excitation and collection geometry

The quantum diamond spectrometer is optimized for electronic and nuclear spin sensing on the diamond surface. The use of a total internal reflection geometry minimizes back-reflection of the laser

into the detector and reduces unwanted exposure of the sample to excitation light. Note that energy can still flow from the laser beam into the sample via the evanescent wave produced at the diamond–sample interface. Total internal reflection can be achieved either by sending the laser through an edge of the diamond or through the light guide into the bottom of the diamond chip (the method depicted in Fig. 4 and used in this protocol). More-glancing angles of incidence can be accessed with through-edge illumination, but this requires polishing of the diamond edge. Excitation through the light guide has the additional disadvantage that high laser power might degrade the glue used to attach the diamond to the light guide over time. The presence of the glue may also increase background fluorescence.

NV fluorescence is collected with an optical light guide (e.g., Edmund Optics), which is glued with optical epoxy to the bottom of the diamond, which in turn guides the collected light onto a large-area avalanche photodiode (APD) for detection. The light-guide diameter should match the size of the diamond. Moreover, the light-guide scheme makes the experiment fairly insensitive to any optical misalignments. Alternatively, a microscope objective can be used instead of a light guide. Compared to the light-guide geometry described here, the use of an objective offers enhanced contrast and spatial resolution at the expense of increased experimental complexity.

Choice of photodetector and interference filter

The photodetector is chosen according to the expected collected photon count rate in a given experiment. Usually, for shallow, high-density implanted NV diamonds, an APD provides the necessary sensitivity and should have a noise equivalent power of <0.1 pW/$\sqrt{Hz}$. The bandwidth is usually limited by the data acquisition (DAQ) unit and is typically >1 MHz. For efficient light collection, the distance between the light guide and the APD surface should be kept as small as possible and the active area of the APD should be larger than the diameter of the light guide. Possible choices of large-area APD include the Luna Optoelectronics SD197-70-72-661 (5-mm active detector diameter, our choice) and SD394-70-72-661 (10-mm active detector diameter) and the Laser Components A-CUBE-S3000-03 (3-mm active detector diameter). For efficient detection of the red fluorescent light and rejection of the green excitation light, a long-pass interference filter (e.g., Semrock BLP01-647R) or an appropriate band-pass interference filter (e.g., SemrockFF01-736/128) should be used. An additional 532-nm notch filter can also be used to further attenuate stray laser light, if desired.

Choice of source of generated pulse sequences

The pulse sequences are generated either by a PulseBlaster (PB) card or an arbitrary waveform generator (AWG). For the applications described in this protocol, a PB card with high temporal resolution is sufficient (e.g., SpinCore PulseBlasterESR PRO 500 MHz). The card should be compatible with the computer used to control the experiment. The PB card generates TTL pulses, which are used both to control the timing of the DAQ unit in the experiment and to switch on and off the laser and MW sources. The latter is accomplished through the use of TTL-controlled RF switches placed in the MW path and in the RF feed path to the AOM. The switches must be rated to handle signals within the relevant frequency ranges (i.e., ~80 MHz for the AOM RF feed and ~1–3 GHz for the MW drive) and must operate with rise times of at most a few nanoseconds (e.g., the Mini-Circuits ZASWA-2-50DR+ switches used in this protocol operate at frequencies ranging from 0 Hz (DC) to 5 GHz and offer rise times that are typically 5 ns and at most 15 ns).

Choice of DAQ unit

The DAQ unit is used to read out the APD voltage. Readout is triggered by TTL signals generated by the PB card and sent to the DAQ unit. The DAQ unit should have a bandwidth that corresponds roughly to the NV repolarization time (in our case ~1 μs). For that reason, we use a DAQ unit with a 700-kHz bandwidth (see specification sheet of our used model); a slower bandwidth will lead to reduced contrast. Our DAQ unit has a sampling rate of 250 kSa/s (thousand samples per second), which sets the maximum repetition time of the experiment (i.e., to 4 μs). The quantum diamond spectrometer described here requires a DAQ unit with at least one analog input (AI) channel and two digital input trigger channels. We use a National Instruments USB-6229 DAQ unit.

Choice of MW source, amplifier, and delivery

Although many options are available, we use a Stanford Research Systems signal source (SG384) with an internal in-phase and quadrature (IQ) mixer for phase control. Any other low-noise and stable signal source in the frequency range 1–4 GHz can also be used in conjunction with external IQ

mixers. The MWs are amplified by a 16-W Mini-Circuits amplifier (ZHL-16W-43+). For MW delivery, we use a loop described in greater detail below. More-sophisticated MW delivery antennas, such as coplanar waveguides or resonators, can also be used[24].

Pulse sequence basics

The NV-based quantum sensing schemes applied in this protocol have previously been described in the literature[13,23,24]. Here, we outline the technical requirements for the implementation of the pulse sequences used in this protocol. In all pulse sequences, the laser and MWs are pulsed on and off on a nanosecond to microsecond timescale. The timing of this pulsing is controlled by a PB card with a 500-MHz clock, which is the heart of the experiment (Fig. 5). The PB card outputs TTL signals to the switches, which control the MW drive (orange) and the laser (blue), via an AOM. Data acquisition with the DAQ is also triggered and gated by the PB. The DAQ unit requires one TTL start trigger (red) that defines the start of the pulse sequence, and a gate trigger (green) that instructs it to acquire data each time a data point is to be collected. For the nuclear spin–sensing pulse sequence, the phase of the MW pulses must also be controlled. This is done here via the IQ option of an SRS SG384 signal generator. The IQ input is controlled by two switches, which are also controlled by TTL signals (brown and violet) generated by the PB. An overview of the pulse sequences used in this protocol is shown in Fig. 6.

NV-ESR pulse sequence

The most basic sequence is the NV-ESR pulse sequence. We distinguish the term NV-ESR from ESR in order to specify that the goal is to obtain a spectrum of the NV spin itself, rather than that of a target sample, using the NV as a sensor. NV-ESR is used to detect the NV resonance frequency and to measure the strength of the applied magnetic field by sweeping the MW frequency f_M and reading out the fluorescence. If the applied MW is on resonance, some population is transferred from $m_s = 0$ to one of the dimmer $m_s = 1$ or $m_s = -1$ states, which causes a dip in the fluorescence signal. In the absence of a strong applied field, usually two resonances can be observed around the zero-field splitting D of 2.87 GHz (Fig. 6a). Upon application of an external field, the lines shift because of the Zeeman effect. If the magnetic field is not aligned along one of the diamond lattice [111] directions corresponding to a particular NV axis, up to eight resonances can be observed in the spectrum of an NV ensemble, which might be further split by hyperfine interactions with a nearby nuclear spin (e.g., nitrogen). This is because each of the four possible NV orientations experiences a different projection of the applied field and thus a different Zeeman shift. If the field is well-aligned along one of the four NV orientations (as it is in this protocol), the two resonances associated with that orientation are maximally shifted from 2.87 GHz. In this case, the applied field has equal projection on the other three NV orientations, causing their resonances to become degenerate. Thus, only four independent resonance frequencies are observed in the spectrum. The NV-ESR sequence is used to determine the NV resonance frequency and the applied magnetic field, which can be calculated approximately according to the following equation:

$$B_0 = \frac{2,870\text{MHz} - f_{NV}(\text{MHz})}{2.8\text{MHz/G}} \quad (6)$$

where f_{NV} is the center of the resonance frequency of the transition at lowest frequency. Keep in mind that D (2.87 GHz) is not an exact constant and might vary depending on temperature and strain in the diamond. This resonance corresponds to the $m_s = 0$ to $m_s = -1$ transition of the NV orientation with the largest magnetic field projection. Usually, the laser light polarization is adjusted by a $\lambda/2$ waveplate to maximize the excitation of this NV orientation. The NV-ESR pulse sequence is shown in Fig. 6a. It requires four PB channels: PB_AOM and PB_MW to control the AOM and MWs, and two channels that act as start (PB_StartTrig) and readout triggers (PB_DAQ) for the DAQ unit. All the pulse sequences used here have two readouts per sequence for low-frequency (< ~50 kHz) noise

Fig. 6 | Overview of the described pulse sequences. a–f, Left side: experimental data. Insets show the basic idea of ▶ the pulse sequence. Right side: pulse sequences and channels programmed into the PulseBlaster card. **a**, ESR experiment at Earth magnetic field (1,000 samples, 1 average). **b**, Rabi experiment at 311 G (1,000 samples, 1 average). **c**, Spin echo experiment at 311 G and 24-ns π pulses (10,000 samples, 1 average). **d**, XY8-1 experiment at 311 G and 24-ns π pulses (10,000 samples, 1 average). **e**, Correlation spectroscopy experiment at 311 G and 24-ns π pulses with τ set to 1.5 μs (10,000 samples, 1 average). **f**, NV-T1 experiment at 311 G with 24-ns π pulses (10,000 samples, 1 average). Samples denote the number of measured points acquired for each data point in the experiment. Averages denote the number of repetitions of the entire experiment.

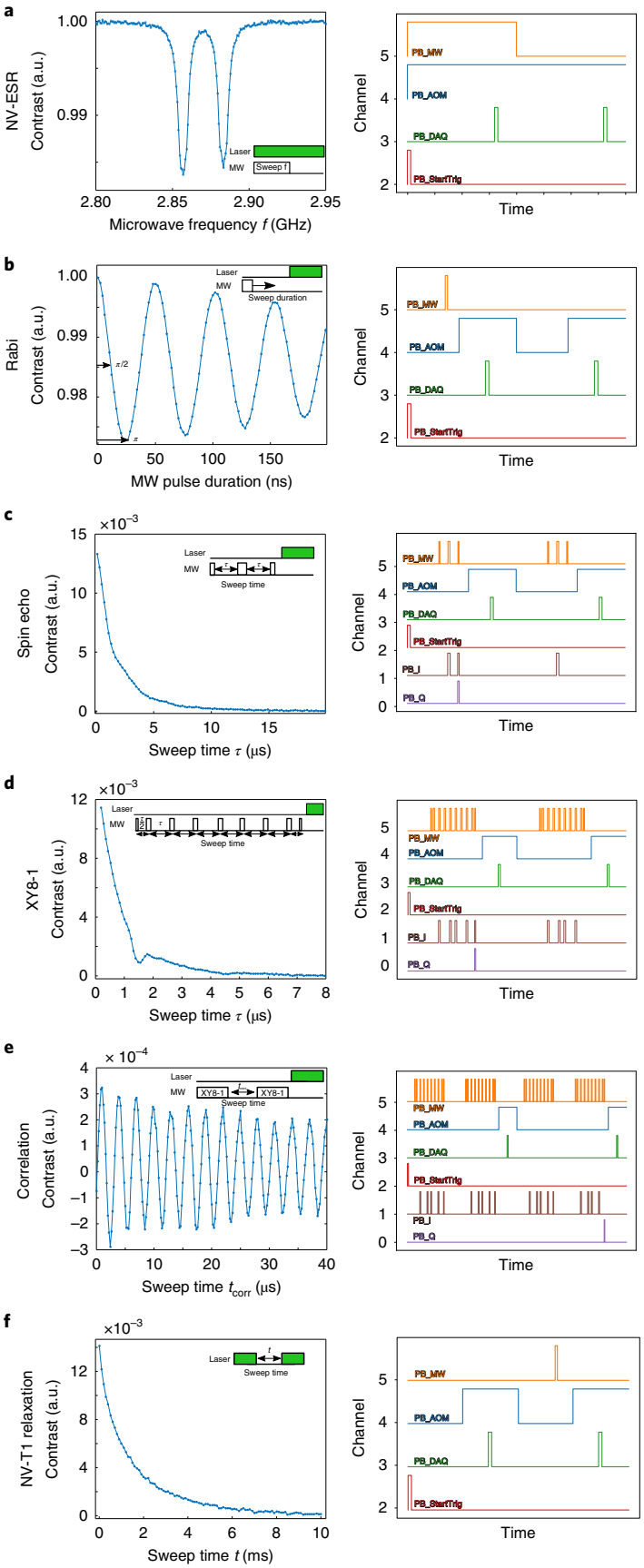
a
NV-ESR
Contrast (a.u.)
1.00
0.99
Laser
MW
Sweep f
2.80
2.85
2.90
2.95
Microwave frequency f (GHz)
PB_MW
PB_AOM
PB_DAQ
PB_StartTrig
Channel
Time
b
Rabi
Contrast (a.u.)
1.00
0.99
0.98
Laser
MW
Sweep duration
π/2
π
0
50
100
150
MW pulse duration (ns)
PB_MW
PB_AOM
PB_DAQ
PB_StartTrig
Channel
Time
c
Spin echo
Contrast (a.u.)
×10−3
15
10
5
0
Laser
MW
Sweep time
0
5
10
15
Sweep time τ (μs)
PB_MW
PB_AOM
PB_DAQ
PB_StartTrig
PB_I
PB_Q
Channel
Time
d
XY8-1
Contrast (a.u.)
×10−3
12
8
4
0
Laser
MW
Sweep time
0
1
2
3
4
5
6
7
8
Sweep time τ (μs)
PB_MW
PB_AOM
PB_DAQ
PB_StartTrig
PB_I
PB_Q
Channel
Time
e
Correlation
Contrast (a.u.)
× 10−4
4
3
2
1
0
−1
−2
−3
Laser
MW
XY8-1
XY8-1
Sweep time
0
10
20
30
40
Sweep time tcorr (μs)
PB_MW
PB_AOM
PB_DAQ
PB_StartTrig
PB_I
PB_Q
Channel
Time
f
NV-T1 relaxation
Contrast (a.u.)
×10−3
12
8
4
0
Laser
Sweep time
0
2
4
6
8
10
Sweep time t (ms)
PB_MW
PB_AOM
PB_DAQ
PB_StartTrig
Channel
Time

cancellation. We refer to the first readout, during which the MW is on, as the 'signal'. The second readout, during which the MW is off, is referred to as the 'reference'. The beginning of the sequence is marked by the DAQ unit start trigger, which prepares the DAQ unit to begin data acquisition. The laser is on during the entire pulse sequence. For each MW frequency f_M, the pulse sequence is repeated $N_{samples}$ (number of samples) times, and so the DAQ unit acquires $2N_{samples}$ data points (signal and reference). The mean of the signal data points is then divided by the mean of the reference data points to give one value of contrast at f_M. After the MW has been swept over all values, the experiment can be repeated for further averaging. The amplitude of the resonance signal depends on MW and laser power, as well as the full duration of the pulse sequence, and should be optimized by the user. Hyperfine interaction with the nuclear spin of the ^{14}N nucleus that comprises part of the NV center splits each resonance into three lines. At high MW power, the lines are broadened and these hyperfine features are obscured.

Rabi pulse sequence

In a Rabi experiment, the MW frequency is tuned to match the NV spin resonance (e.g., to the $m_s = 0$ to $m_s = -1$ transition) and the NV fluorescence is measured as a function of the MW pulse duration. As the NV quantum state undergoes nutation, the expected number of detected fluorescence photons oscillates (Fig. 6b). This Rabi oscillation is measured to determine the durations of $\pi/2$ and π pulses, which are needed for the sensing sequences later. The Rabi frequency can be tuned by changing the MW power. Typical π-pulse durations achieved with the suggested amplifier and loop are ~20–60 ns. The Rabi contrast (fractional difference in signal measured at zero applied MW pulse duration and at π-pulse duration) can be as high as 30% for a single NV. For an ensemble of NVs, the contrast is reduced because of the presence of fluorescence background from off-axis NV centers as well as heterogeneity in NV properties, resulting in typical values in the range of 1–6%. The contrast depends on the degree of NV repolarization (related to laser intensity) and on the presence of other sources of background light (e.g., light scattering, non-aligned NV centers). Obtaining a high contrast is important because sensitivity improves linearly with contrast.

The Rabi pulse sequence requires four PB channels: PB_AOM, PB_MW, PB_DAQ, and PB_StartTrig. The AOM polarization and readout pulse are usually combined in one pulse. The first part (~1 μs) of the AOM pulse is used to read out the NV state, whereas the subsequent 4 μs repolarize the NV. These durations depend on the laser intensity and must be optimized in each case. We use a laser intensity of ~10 kW/cm^2. The timing of the DAQ unit readout pulse relative to the AOM pulse must be chosen carefully. Early readout leads to a reduction of signal-to-background because the population transfer may be probed before completion of the MW pulse sequence. Late readout results in a signal-to-background reduction because most of the information about the NV population is lost once the laser has been on long enough to produce significant repolarization. Although the PB outputs the AOM and DAQ unit trigger pulses at the same time, the arrival times of these pulses are usually delayed with respect to each other because of the non-negligible AOM response and/or differences in cable lengths. For that reason, the DAQ unit readout pulse output of the PB is manually delayed in order to properly synchronize the AOM and DAQ unit readout pulses. As with the NV-ESR sequence, the second half of the pulse sequence is the reference readout (without MW manipulation) for noise cancellation.

Spin-echo (Hahn-echo) NV-T2 relaxation pulse sequence

The most basic AC magnetometry sequence is the spin-echo (Hahn-echo) sequence. It consists of a sequence ($\pi_x/2-\tau-\pi_y-\tau-\pi_{x(-x)}/2$) of MW pulses separated by free precession time τ. As τ is swept, the signal decays according to the transverse relaxation of the NV with time constant NV-T2$_{Hahn\text{-}echo}$. τ should be much longer than the π-pulse duration (we typically use pulse durations of $\tau > 4\pi$ *pulse durations*). In addition to the four standard PB channels (PB_AOM, PB_MW, PB_DAQ, and PB_StartTrig), two additional channels are needed to control the phase of the MW pulses. Four possible on/off combinations of these two pulses determine the phase output of an IQ mixer (Table 1). The I and Q pulses should be longer than the MW pulses in order to compensate for the finite response time of the IQ mixer.

For common noise cancellation, the pulse sequence is applied twice. In the second sequence, the last $\pi/2$ pulse of the spin-echo is phase-shifted by 180° relative to the last $\pi/2$ pulse of the first

Table 1 | IQ modulation

I channel	Q channel	Rotational axis	Phase shift
Off	Off	x	0°
On	On	$-x$	180°
On	Off	y	90°
Off	On	$-y$	270°

sequence. With these two readouts (R_1 and R_2), the contrast (C) can be calculated according to:

$$C = \frac{R_1 - R_2}{R_1 + R_2} \quad (7)$$

Keep in mind that this contrast definition is different from that in the ESR and Rabi experiments. We plot contrast versus free precession time for a spin-echo measurement in Fig. 6c. In addition to the described decay, two shallow dips can be observed. These are caused by ^{13}C spins located within the diamond lattice, which precess at $f = 330$ kHz at 311 G. The first dip occurs at $\tau = 1.5\ \mu s = 1/(2f)$, whereas the second dip occurs at a harmonic: $\tau = 4.5\ \mu s = 3/(2f)$.

For high-density, shallow NV ensembles, the NV-T2$_{\text{Hahn-echo}}$ time is typically around a few microseconds. NV-T2$_{\text{Hahn-echo}}$ is an important parameter, because it sets the lowest frequency that can be sensed. Usually the NV-T2$_{\text{Hahn-echo}}$ time is extended for higher sensitivity through the application of trains of π−pulses in dynamic decoupling sequences, e.g., an XY8-N sequence as described in the following paragraph.

XY8-N dynamical decoupling pulse sequence

The XY8-N sequence consists of trains of pulses of the following form: $\pi_x/2-\tau/2-(\pi_x-\tau-\pi_y-\tau-\pi_x-\tau-\pi_y-\tau-\pi_y-\tau-\pi_x-\tau-\pi_y-\tau-\pi_x)^N-\tau/2-\pi_{x(-x)}/2$. For $N = 1$, the sequence consists of a train of 8 π pulses in which the rotation axis is alternated between x and y (Fig. 2) in order to partially compensate for pulse errors[25,26]. Note that the $\pi/2$ and π pulses are separated by time $\tau/2$ and that the spacing between consecutive π pulses is τ. Sweeping τ and monitoring the fluorescence reveals a decaying contrast. The decay timescale is extended compared to that obtained when a simple Hahn-echo pulse sequence is applied[55] (Fig. 6d). To plot the data on a real-time axis, remember to scale the scanned parameter axis τ by $8{\cdot}N$. The dip at $\tau = 1.5\ \mu s$ observed in the data is caused by ^{13}C precession at the Larmor frequency f_L, which fulfills the condition $1/(2f_L) = \tau$. The dip is more pronounced in the XY8-N than in the Hahn-echo experiment because more phase is accumulated and the sharper filter function narrows the line. Using more π pulses (higher N) intensifies these effects. However, N is ultimately limited by the NV-T2 (i.e., there is a reduction in contrast as the pulse sequence duration increases). In addition, pulse errors accumulate over long dynamic decoupling sequence, which reduces the contrast. For that reason, the optimum N must be found experimentally. The pulse sequence requires the same number of PB channels (PB_AOM, PB_MW, PB_DAQ, PB_StartTrig, PB_I (to control the I channel of the IQ mixer), and PB_Q (to control the Q channel of the IQ mixer)) and implements the same noise-cancellation scheme (Eq. 7) as the Hahn-echo sequence.

Correlation spectroscopy pulse sequence

The correlation spectroscopy pulse sequence consists of two XY8-N sequences separated by t_{corr}: $\pi_x/2-\tau/2-(\pi_x-\tau-\pi_y-\tau-\pi_x-\tau-\pi_y-\tau-\pi_y-\tau-\pi_x-\tau-\pi_y-\tau-\pi_x)^N-\tau/2-\pi_y/2\text{-}t_{corr}-\pi_x/2-\tau/2-(\pi_x-\tau-\pi_y-\tau-\pi_x-\tau-\pi_y-\tau-\pi_y-\tau-\pi_x-\tau-\pi_y-\tau-\pi_x)^N-\tau/2-\pi_{y(-y)}/2$. Note that the phase of the last $\pi/2$ pulse of each XY8-N sequence is shifted 90°/270° relative to the first $\pi/2$. The time t_{corr} between these two sequences is swept and the fluorescence recorded. The π-pulse spacing τ in the XY8-N sequences is set to satisfy the condition $\tau = 1/(2f_0)$, where f_0 is the frequency of the signal we want to sense (and τ is the time at which the dip in the XY8-N decay occurs). The recorded data oscillate at the signal frequency f_0. In the example of Fig. 6e, we sense the ^{13}C NMR signal in diamond by setting τ to 1.5 μs, which results in an oscillation at 330 kHz (f_L). To resolve the Larmor frequency, the sampling of t_{corr} should be high enough to provide at least two points per signal-field period ($1/f_0$), and more may be preferable for straightforward analysis of the data. Of course, the full oscillation can be undersampled

in order to speed up acquisition if the experimenter has sufficient prior information about the target frequencies to resolve potential ambiguities. As in the previously described experiments, low-frequency noise is cancelled by imposing a 180° phase shift between the last $\pi/2$ pulses of two successive correlation spectroscopy sequences (Eq. 7). As with the XY8-N sequence, N should be optimized to find the highest signal-to-noise ratio (SNR).

NV-T1 relaxation pulse sequence

The NV-T1 relaxation pulse sequence is very simple and, in principle, requires no MW pulses. To measure NV-T1 (longitudinal) relaxation, the time t between AOM laser pulses is swept. As in all previous pulse sequences, the readout AOM pulse and repolarization AOM pulse are combined. By sweeping the total sequence duration t, the fluorescence decays exponentially according to the longitudinal relaxation of the NVs from the polarized $m_s = 0$ state into the thermal equilibrium mixed state (Fig. 6f). For low-frequency noise cancellation, the pulse sequence is repeated, but the relaxation from $m_s = 1$ to the thermal state is measured by applying a π pulse on the NV after optical polarization. The contrast is calculated according to Eq. 7. The pulse sequence requires four PB channels: PB_AOM, PB_MW, PB_DAQ, and PB_StartTrig. Typical NV-T1 relaxation times for NVs at room temperature are a few milliseconds.

Materials

! CAUTION Ensure that all chemicals, substances, equipment, and apparatus in this protocol are handled and operated safely by obtaining, reading, and following their respective manufacturers' safety instructions. **▲ CRITICAL** We list the equipment used for our experimental setup. Unless otherwise specified, items can be replaced by equivalent components from other vendors with similar performance.

Reagents

Samples

- Polydimethylsiloxane for ^{1}H sensing (PDMS; Sylgard 184; Sigma-Aldrich, cat. no. 761028)
- Fomblin oil for ^{19}F sensing (Sigma-Aldrich, cat. no. 317993-100G)
- Copper (II) sulfate pentahydrate for transition metal sensing (Sigma-Aldrich, cat. no. 31293)

Acid clean reagents

- Deionized (DI) water (Sigma-Aldrich, cat. no. 1026991000)
- Isopropyl alcohol (IPA; Sigma-Aldrich, cat. no. 59304)
- Sulfuric acid (Merck, cat. no. SX1244-6) **! CAUTION** Sulfuric acid is strongly corrosive. Protective equipment should be worn (laboratory coat, gloves, safety goggles), and all handling should be performed in a ventilated laboratory fume hood).
- Nitric acid (EMD Millipore, cat. no. NX0409-4) **! CAUTION** Nitric acid is strongly corrosive and oxidizing. Protective equipment should be worn (laboratory coat, gloves, safety goggles), and all handling should be performed in a ventilated laboratory fume hood).
- Perchloric acid (VWR, cat. no. BDH4550-500ML) **! CAUTION** Perchloric acid is strongly corrosive and oxidizing. Protective equipment should be worn (laboratory coat, gloves, safety goggles), and all handling should be performed in a ventilated laboratory fume hood).

Equipment

General equipment

- Oscilloscope (Keysight, model no. DSO7104A)
- Signal source for coil signals (Rigol Technologies, cat. no. DS1022)
- Voltmeter (Fluke, model no. 77 IV)
- Optical power meter for measuring laser intensity (Thorlabs, model nos. PM100D and S121C)
- Laser goggles (Thorlabs, model no. LG3)
- RF power meter (Keysight, cat. no. V 3500).
- Soldering iron and solder (DigiKey, cat. no. T0052919099N-ND)
- Epoxy glue (optical epoxy; Epoxy Technology, cat. no. 301-2 KIT)
- Instant adhesive (Krazy Glue).
- Thermal paste (Arctic Silver, Arctic Silver 5 or Arctic Alumina) **! CAUTION** Consult the safety data sheet for handling.

Cables
- BNC cables (Thorlabs, cat. no. 2249 series)
- SMA cables (Thorlabs, cat. no. CA 2912)
- BNC/SMA adaptors (i.e., a selection of BNC–SMA, SMA–SMA, and BNC–BNC adaptors for all gender combinations; e.g., Thorlabs, cat. nos. T4291, T4290, T4289, T4288, T4285, T4283, T3283 and T3533)

Acid clean equipment
- Round-bottom flask (one; 25 mL; Chemglass, cat. no. CG-1510-32)
- Reflux condenser that fits with round-bottom flasks, stand, and clamps (Chemglass, cat. no. CG-1215-A-10)
- Gas bubbler that fits to the reflux condenser (Chemglass, cat. no. AF-0513-20)
- Heating mantle for the round-bottom flasks (Chemglass, cat. nos. CG-14000-04 and CG-15005-01)
- Beakers (10 mL. 50 mL and 100 mL; Chemglass, cat. nos. CG-8048-10, CG-8048-50 and CG-8048-100)
- Cleanroom cups (Cole-Parmer, cat. no. UX-06200-08)
- Ceramic tweezers (Ted Pella, Inc, cat. no. 5029-3 or EMS, cat. no. 78127-71)
- Nitrogen gas blower (Airgas, model no. NI UHP200)

Recommended protective equipment
- Nitrile gloves (VWR, cat. no. 10769-364)
- Lab coat (VWR, cat. no. 10141-342)
- Acid gloves (VWR, cat. no. 32916-240)
- Face shield (VWR, cat. no.14230-968)

Diamond substrate
- Electronic-grade diamond substrate (Element Six, cat. no. 145-500-0385)

Diamond annealing equipment
- Oven apparatus: oven and heating controller (Applied Test Systems, series 3210)
- Quartz tube (Finkenbeiner Inc, custom order: length: 16 inches; o.d., 1.5 inches; i.d., 1.34 inches, one end should be sealed)
- ConFlat (CF) to quick-connect coupling (Kurt J. Lesker, cat. no F0275XVC150)
- Gate valve (Huntington, cat. no. GVA-150-C)
- Turbo pump (Pfeiffer, cat. no. TMU071 P)
- Roughing pump (Pfeiffer, cat. no. MVP-015 T)
- Vacuum gauge (Pfeiffer Vacuum, cat. no. D-35614 Asslar)
- Miscellaneous 2-3/4 inch CF Connectors: tees, elbows, crosses (Kurt J. Lesker, cat. nos. T-0275, L-0275 and C-0275)
- Quartz boat (MTI, cat. no. EQ-QB-1042)
- Copper gasket (oxygen-free high-thermal-conductivity (OFHC) copper gaskets for CF flanges; flange o. d., 2–3/4 inches; Kurt J. Lesker, cat. no. GA-0275)

Laser
- Continuous-wave laser (532 nm; with ~1-W or higher output; Coherent, Verdi G series)

! CAUTION Exposure of the eyes or skin to the laser can be harmful. Use appropriate laser goggles and follow the general laser safety guidelines.

Optics and optomechanics for the quantum diamond spectrometer
- Optical table (one; Thorlabs)
- Opto-mechanics for mounting freestanding optics (we recommend Thorlabs, cat. nos. ESK01, ESK16 and ESK22)
- Long-pass interference filter (650 nm; Semrock, cat. no. BLP01-647R) or suitable band-pass filter (Semrock, cat. no. FF01-736/128); optional 532 notch filter (Semrock, cat. no. NF01-532U-25)
- *XY*-translation stage with a rotating platform (one; Thorlabs, cat. no. XYR1)
- Translation stage (one; 1 inch; Thorlabs, cat. no. PT1)
- Manual rotation stage (one; 2-inch diameter; Thorlabs, cat. no. RP01)
- Travel single-axis translation stages (two; 1/4 inch; Thorlabs, cat. no. MS1S)
- Pedestal pillar posts (four; 1.5 inches; Thorlabs, cat. no. RS1.5P)

- Pedestal pillar posts (two; 3 inches; Thorlabs, cat. no. RS3P)
- Pedestal post holder (one; 1 inch; Thorlabs, cat. no. PH082E)
- Aluminum posts (two; 0.75 inches; Thorlabs, cat. no. TRA075)
- Aluminum posts (two; 1 inch; Thorlabs, cat. no. TRA1)
- Posts (three, 1.5 inches; Thorlabs, cat. no. TR1.5)
- Posts (three, 1 inches; Thorlabs, cat. no. TR1)
- Mini-series mounting posts (two; 2 inches; Thorlabs, cat. no. MS2R)
- Mini-series mounting posts (two; 1 inch; Thorlabs, cat. no. MS05R)
- Base plate (one; Thorlabs, cat. no. PT101)
- Right-angle bracket (one; Thorlabs, cat. no. PT102)
- Dovetail rail carriers (two; Thorlabs, cat. no. RC1)
- Dovetail optical rail (one; Thorlabs, cat. no. RLA1200)
- Compact kinematic mirror mounts (two; Thorlabs, cat. no. KMS)
- Fixed 90° brackets (four; Thorlabs, cat. no. ER90B)
- Cage adaptor plate (one; Thorlabs, cat. no. SP05)
- Removable cage plate (one; Thorlabs, cat. no. CP90F)
- Mounting base (one; Thorlabs, cat. no. BA2)
- Swivel post clamp (one; Thorlabs, cat. no. MSWC)
- Angle clamps (one; Thorlabs, cat. no. RA90)
- Right- angle end clamps (four; Thorlabs, cat. no. RA180)
- Stackable lens tube (one; 1/2-inch diameter; Thorlabs, cat. no. SM05L03)
- Adaptor with external SM1 threads and internal SM05 threads (one; Thorlabs, cat. no. SM1A6T)
- SM1-threaded adaptors with smooth internal bore (one; 16-mm diameter; Thorlabs, cat. no. AD16F)
- Mount for a 4-mm × 25-mm light pipe (one; Edmund Optics, cat. no. 64-907)
- Hexagonal light pipe (light guide; 4-mm aperture, 50-mm length; one; Edmund Optics, cat. no. 49-402)
- Dovetail translation stage with baseplate (one; Thorlabs, cat. no. DT12XYZ)
- Lens with a focal length of 50 mm (one; 30 mm; Thorlabs, cat. no. LA1289-A)
- Set screws (8-32; Thorlabs, cat. nos. HW-KIT2 and HW-KIT3)
- Set screws (1/4-inch, 20; Supplier, cat. no. XXXXXX)
- Lens mount (holder; Thorlabs, cat. no. LMR05)

Photodetector

- Large-area APD (Luna Optoelectronics, cat. no. SD197-70-72-661); it requires an additional power supply with +12, −12 V, and ground (GND) outputs in addition to +5 V and GND for the onboard cooling element. For details, consult the APD manual. We use an additional heat sink and a small fan to further facilitate heat dissipation.

MW parts

- Signal generator (one; SRS, cat. no. SG384; this is an MW signal generator with an IQ option) ▲ **CRITICAL** The qdSpectro software package[56] used in this protocol is designed to work with an SRS SG384 signal generator and has been tested only with this and the SG386 models. It should be compatible with other SRS models (SG3800 or SG3900) but has not been tested with these. Other pulse generators can be used, but these will require modification of the qdSpectro code by the user.
- USB/GPIB converter (one; National Instruments, cat. no. GPIB-USB-HS)
- High-power amplifier (one; Mini-Circuits, cat. no. ZHL-16W-43+)
- Circulator (DiTom, cat. no. D3C2040)
- Parts for MW loop: SMA straight solder Plug (Amphenol, cat. no. 901-9867-RFX) and semi rigid coaxial cable (Micro-Coax, cat. no. UT-047C-TP)
- Loop mounting: table clamp (Thorlabs, cat. no. CL5), right-angle clamp (Thorlabs, cat. no. RA90) and SMA female adaptor (Thorlabs, cat. no. T4285)
- Attenuators (BNC, 50 Ω; Minicircuits, cat. no. HAT series)
- Type N male to SMA female adaptor (to connect SMA cable to RF output of SRS SG384 signal generator; DigiKey, part no. ADAPT/N-TYPEM/SMAF-ND)

Pulsing source

- PB card (500 MHz; SpinCore, cat. no. PBESR-PRO-500) ▲ **CRITICAL** The qdSpectro software package used in this protocol has been tested only with this card but should be compatible with other SpinCore PB cards. Other signal generators can be used but will require modification of the qdSpectro code by the user.

- MW switches (four; Mini-Circuits, cat. no. ZAWSA-2-50DR+)
- Subminiature version A (SMA) 50 Ω coaxial terminators/loads (four; Amphenol, cat. no. 132360)
- T connector (Digikey, part. no. ACX1433-ND)

AOM and optics for the laser path

- AOM (80 MHz; IntraAction, model no. ATM-801A2) with 80-MHz AOM driver (IntraAction, model no. ME-802N)
- Opto-mechanics for mounting freestanding optics (Thorlabs, cat. nos. ESK01, ESK16 and ESK22)
- Lenses (one each of focal length 50, 100, 200, and 400 mm; Thorlabs, cat. nos. LA1131-A-ML, LA1509-A-ML, LA1708-A-ML, and LA1172-A-ML)
- Pinhole (200 μm; Thorlabs, cat. no. P200H) and translating lens mount (Thorlabs, cat. no. LM1XY)
  ▲ **CRITICAL** Choice of exact pinhole size depends on required extinction ratio.
- Five-axis aligner (Newport, cat. no. 9081-M)
- Pedestal post holder (one; 1 inch; Thorlabs, cat. no. PH082E)
- Optical post (1 inch; Thorlabs, cat. no. TR1V)
- Iris (Thorlabs, cat. no. IDA12-P5)
- Waveplate (λ/2; Thorlabs, cat. no. WPH05M-532) in a continuous-rotation mount (Thorlabs, cat. no. RSP1)
- Protected silver mirrors (five; 1-inch diameter; Thorlabs, cat. no.PF10-03-P01), mounted in precision kinematic mirror mounts (Thorlabs, cat. no. KM100). Note that the number of mirrors depends on the experiment and space restrictions.

Magnets

- Static magnets with a diameter of >1 cm (two samarium–cobalt magnets; Electron Energy Cooperation, cat. no. EEC 2:17-TC-17). We stack two of these magnets in order to increase the magnetic field strength and homogeneity.

Power supplies

- Power supply for powering MW switches and for powering APD cooling element (±5 V; Newark, cat. no. 56AC4684)
- Power supply for powering MW amplifier (28 V/4.3 A; Newark, cat. no. 56AC4684)
- Power supply for powering APD (±12 V; Newark, cat. no. 56AC4684)
- Power supply for powering IQ modulation of the SRS SG384 (±0.35 V; Newark, cat. no. 56AC4684)

DAQ unit

- DAQ card with a sampling rate of at least 250 kSa/s (National Instruments, cat. no. NI USB-6229 or NI USB-6211) ▲ **CRITICAL** The qdSpectro software package used in this protocol was tested with the NI USB-6229 and NI USB-6211 models. The code is designed to work with National Instruments DAQ units and will require modification by the user if other data acquisition systems are used.

Computer

- Personal computer (PC); the software installation is described in the protocol for a Windows PC and the qdSpectro package has been tested with Windows 10. It should be portable to Linux or Mac operating systems but has not been tested in these platforms and may require some user modification. (At the time of writing, system requirements are: at least 1 GHz processor speed, a DirectX 9 or later graphics card with WDDM 1.0 driver and, for 64-bit processors, at least 2 GB RAM and 20 GB hard disk space or, for 32-bit processors, at least 1 GB RAM and 16 GB hard disk space.)

Software packages

▲ **CRITICAL** Recommended installation procedures for the software used in this protocol are described in the Procedure in Steps 18–32. Below, the necessary packages, libraries, and drivers are listed for reference.

- qdSpectro[56] (this is a Python package developed to run the experiments described in this protocol. It can be downloaded from https://gitlab.com/dplaudecraik/qdSpectro or https://doi.org/10.5281/zenodo.1478113. The current version at the time of writing is v.1.0.1, but the user is encouraged to download the latest version. The package includes a readme file, which users should refer to for any patches or updates, as well as a list of software dependencies (including version numbers with which the package has been tested))

- Python v.3 (v.3.6.3 or later and of a bitness that matches the computer's bitness (i.e., install 64-bit Python if will be running on a 64-bit computer): https://www.python.org/)
- Notepad++ or any other text editor of your choice for viewing and editing Python scripts (https://notepad-plus-plus.org/)

Drivers

- National Instruments NI-DAQmx driver compatible with your chosen DAQ card and operating system (https://www.ni.com/dataacquisition/nidaqmx.htm)
- National Instruments drivers for the USB/GPIB converter used for GPIB communication between the PC and the SRS signal generator. qdSpectro has been tested with the National Instruments GPIB-USB-HS converter, which requires the NI-VISA (https://www.ni.com/visa/) and NI-488.2 (https://www.ni.com/en-us/support/downloads/drivers/download.ni-488-2.html#305442) drivers to be installed
- SpinAPI package: SpinCore API and Driver Suite for the PB card (http://www.spincore.com/support/spinapi/SpinAPI_Main.shtml)

Libraries for peripheral instrument control

- SpinAPI Python3 wrapper: SpinCore's Python wrapper for C functions in SpinAPI, which can be used to communicate with and control the PB card (http://www.spincore.com/support/SpinAPI_Python_Wrapper/Python_Wrapper_Main.shtml; accessed 25 July 2019). If the aforementioned link is no longer active, the required version of spinapi.py can still be retrieved at https://web.archive.org/web/20190208140542/ by copying the following link into the search window: http://www.spincore.com/support/SpinAPI_Python_Wrapper/spinapi.py
- NI-VISA library: this library will probably be included with the drivers for the NI GPIB/USB converter, but, if not, it can be separately obtained by selecting the chosen version of NI-VISA from the drop-down menu (qdSpectro has been tested with version 16.0) and clicking the download button. It is an implementation of the virtual instrument software architecture (VISA) application programming interface (API). The VISA API facilitates communication with peripheral instruments and must be installed to enable qdSpectro to communicate with the SRS signal generator via GPIB. The bitness of this library must match the Python bitness
- PyVISA v.1.8 or later: a Python wrapper for the NI-VISA library, which allows the library to be called from Python scripts; https://pypi.python.org/pypi/PyVISA

Python libraries for data manipulation and graphical display

- Matplotlib: a Python library for plotting (https://matplotlib.org/index.html)
- NumPy: a Python library for scientific computing (http://www.numpy.org/)

Procedure

Fabrication of NV diamond chips ● Timing 2 d

! CAUTION Ensure that proper protective equipment (acid gloves, face shield, and lab coat) is worn during the cleaning procedure. Institutional protocols should be followed regarding waste and chemical usage. The cleaning procedure must be performed in a fume hood. Chemical-resistant ceramic tweezers should be used to avoid damaging the diamond surface or chipping edges.

▲ CRITICAL Acid cleaning (Steps 1–11) is recommended before sending the diamond out for implantation, before and after annealing, and generally to remove residue from the surface or before changing to a new sample.

1 *Acid cleaning (Steps 1–11).* Set up a round-bottom flask, reflux condenser, and bubbler on the heating mantle as shown in Fig. 7. Connect cooling water to the reflux condenser. Fill the bubbler halfway with water and connect it to a weak air flow.
! CAUTION This is important to prevent leakage of acid fumes, because perchloric acid fumes are explosive.

2 Transfer the diamonds to the round-bottom flask.

3 Pour 5 mL of sulfuric acid into a beaker. Add 5 mL of perchloric acid to the beaker. Add 5 mL of nitric acid. The order in which you pour acids is related to fuming. Nitric acid fumes the most and sulfuric the least. Pour this tri-acid solution into the round-bottom flask with the diamonds.

4 Insert a condenser into the round-bottom flask and turn the heating mantle on to boil the acids. Keep the fume hood closed. Keep the acid solution boiling for 1 h. After 1 h, turn the heater off and let the solution cool for 30 min.

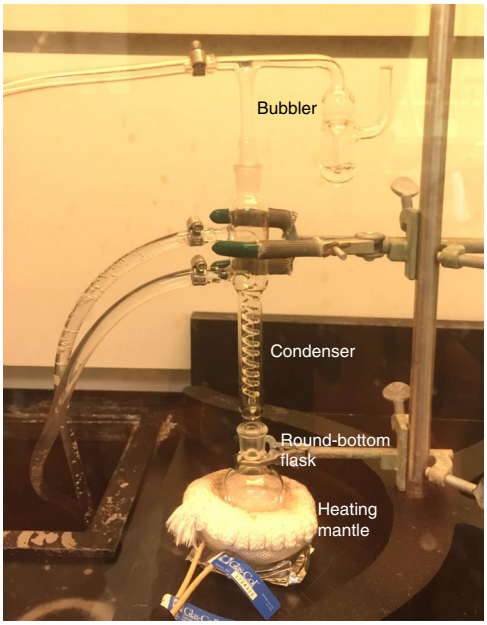

Fig. 7 | Setup of the glassware for acid cleaning.

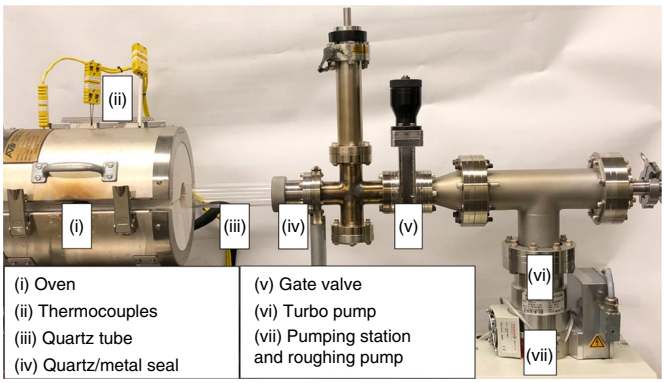

Fig. 8 | Vacuum furnace system for diamond annealing.

5 Prepare a beaker with DI water for diluting the acid residue.

6 Lift the condenser out of the flask. Pour the majority of the acid out of flask into the proper waste container.

▲CRITICAL STEP Be careful not to pour the diamonds out of the flask during this process.

7 Begin the dilution process. Pour DI water into the round-bottom flask and swirl it around to dilute the acid residue. Pour wastewater from the flask into a waste container (again making sure not to pour the diamonds out). Repeat this step at least twice.

8 Fill the flask with DI water and pour all of the contents of the flask (including the diamonds) into a cleanroom cup, or a similarly clean container. Repeat this step until all diamonds are removed from the flask.

9 Using ceramic tweezers, transfer the diamonds from the DI water to a cup of IPA solution.

10 Dry the diamonds with a nitrogen gas blower and put them into a clean container for storage.

11 Properly rinse all glassware and dispose of all chemical waste in the correct containers.

■PAUSE POINT The diamonds can be stored in a clean container and either used for quantum sensing experiments (nitrogen implanted diamond) or sent out (substrates) for ion implantation. After implantation, the diamond must be cleaned (Steps 1–11) again before proceeding with the annealing (Steps 12–17). Diamonds should be stored at room temperature (15–30 °C). Diamonds can be stored for approximately several weeks without needing further cleaning.

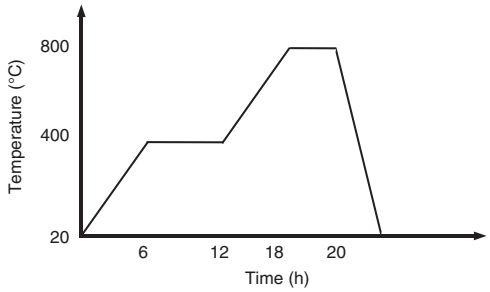

Fig. 9 | Example heating profile for diamond annealing.

12 *Annealing (Steps 12–17).* Retrieve quartz boat and quartz tube from clean storage locations. Place the quartz boat in an enclosed space (to avoid losing the diamond if it is dropped while being transferred). Use ceramic tweezers to transfer the diamond samples (several samples can be annealed at once in this configuration) to the quartz boat. Place the quartz boat back into the quartz tube and push the quartz boat down to the end of the quartz tube (into the area that will be under the furnace).

▲ **CRITICAL STEP** The annealing procedure (Steps 12–17) should be done after the diamonds have been implanted with ions and acid-cleaned. The procedure described here is for use with an in-house-built vacuum furnace system (Fig. 8). Owing to the complexity of setting up an annealing system, we advise either sending out the diamond sample to another research group with a working furnace or using a commercial option (e.g., http://www.laserage.com/heat-treating). Similar procedures and considerations are applicable to analogous systems. Steps 12–17 are for a starting condition in which the furnace is not under vacuum and has been opened and the turbo pump has been spun down.

13 Use a CF flange to seal the quartz tube to the rest of the vacuum assembly. Place a copper gasket between the two metal seals, making sure that it is in the proper place relative to the knife edge. Ensure the quality of the vacuum seal through proper tightening of the bolts and nuts for the seal.

14 Open the gate valve. The roughing pump will begin pumping down the entire chamber. Consult the manual of the turbo pump being used to determine the minimum pressure needed to spin the turbo pump up to speed. Once this pressure is reached, turn on the turbo pump and wait for the chamber pressure to decrease. The wait time depends on the turbo pump used and the volume of the vacuum chamber. Once the pressure reaches an acceptable level ($<10^{-7}$ mbar), then one is ready to start the heating.

15 Program the heating profile (Fig. 9) into the furnace controller. Ramp from room temperature to 400 °C over 6 h. Hold at 400 °C for 6 h. Ramp from 400 °C to 800 °C over 6 h. Hold at 800 °C for 2 h.

16 Let the furnace cool to room temperature. Close the gate valve and spin down the turbo pump. Unseal the quartz tube from the furnace.

■ **PAUSE POINT** The diamonds can be stored in a clean container.

17 Acid-clean the diamonds as described in Steps 1–11.

Construction of the quantum diamond spectrometer ● Timing 3 weeks

▲ **CRITICAL** The following steps (18–49) are necessary only for the initial construction of the setup. If you are using an existing setup, proceed to Steps 50–58.

18 *Installation of experimental-control software (Steps 18–25).* Download and install Python 3 v.3.6.3 or later from https://www.python.org/. The Python bitness must match both the NI-VISA library's bitness (Step 20) and the computer's/operating system's bitness. This protocol describes how to run Python scripts from a Windows command prompt and how to edit the scripts using Notepad++, a text editor. The user may opt to run and edit the scripts from an Integrated Development Environment (IDE) instead, or to use a different editor.

19 To check that the Python installation was successful, run Python by typing `python` into a Windows command prompt and pressing 'Enter'. This should return the Python version number and bitness. To exit Python, type `exit()` (or hold down the 'Ctrl' key and press the 'z' key), followed by 'Enter'.

20 Download and install the required drivers for the NI USB/GPIB converter (NI GPIB-USB-HS converter). These drivers should include the NI-VISA library, but, if not, the library can be

separately obtained (by selecting the chosen version of NI-VISA) from the drop-down menu (qdSpectro has been tested with version 16.0) and clicking the download button).

From a Windows command prompt, install pyVISA by running the following command:

```
python -m pip install -U pyvisa
```

Check that the library was successfully installed by starting Python (by typing `python` into the command prompt and pressing 'Enter', as in Step 19) and then running

```
import visa
```

If no errors appear, the installation was successful.

▲ **CRITICAL STEP** Ensure that the bitness of the NI-VISA library matches the Python bitness (i.e., install 64-bit NI-VISA if running it on a 64-bit operating system).

21 From a Windows command prompt, install matplotlib by running the following command:

```
python -m pip install -U matplotlib
```

Check that the library was successfully installed by starting Python and then running the following command:

```
import matplotlib
```

If no errors appear, the installation was successful.

22 From a Windows command prompt, install NumPy by running the following command:

```
python -m pip install -U numpy
```

Check that the library was successfully installed by starting Python and then running the following command:

```
import numpy
```

If no errors appear, the installation was successful.

23 Download and install Notepad++ from https://notepad-plus-plus.org/.

24 Choose a folder in which to install qdSpectro, the package containing the Python scripts needed to run the experiments described in this protocol. This folder is henceforth referred to as the working directory. Download qdSpectro from https://gitlab.com/dplaudecraik/qdSpectro and save it in the working directory (see Box 1 for a brief description of files included in the package). The current package version at the time of writing is v.1.0.1, but users are encouraged to download the latest version. Users should check the readme file of the package for any patches and version-specific changes to the instructions given in this paper.

25 Download the SpinAPI Python Wrapper from http://www.spincore.com/support/SpinAPI_Python_Wrapper/Python_Wrapper_Main.shtml (if this link is no longer active, the required version of spinapi.py can still be retrieved from https://web.archive.org/web/20190208140542/ by pasting the following into the search window: https://web.archive.org/web/20190208140542/http://www.spincore.com/support/SpinAPI_Python_Wrapper/spinapi.py).

▲ **CRITICAL STEP** Save the file as spinapi.py in the working directory.

26 *PB and DAQ unit setup (Steps 26–32)*. Follow the instructions in the 'Installation' section of the PB manual (e.g., page 9 of the PulseBlasterESR-PRO manual version from 4 September 2017). This includes downloading the SpinAPI package, inserting the PB card into an available peripheral component interconnect (PCI) slot in the computer and testing the PB using one of the test programs SpinCore provides.

27 Follow the installation instructions for the National Instruments DAQ unit (e.g., chapter 1 of the NI USB-621x manual version from April 2009 (https://www.ni.com/pdf/manuals/371931f.pdf). This includes downloading the NI-DAQmx driver and connecting the DAQ card to the computer via USB.

28 Refer to the analog input (AI) section of the DAQ unit manual (e.g., chapter 4 in the NI USB-621x manual version from April 2009) for a description of the available connection modes for AI signals.

Box 1 | Using the qdSpectro package

Once the qdSpectro package has downloaded, the working directory should contain the files listed below.

User-input configuration files

- connectionConfig.py: configuration file for the PB, DAQ unit, and SRS connections to the PC. This file is edited by the user, as directed in the protocol, before any of the package scripts are run.
- Other [variable text]config.py files: experiment configuration files. Each experiment has its own configuration file (e.g., the configuration file for the ESR experiment is ESRconfig.py), which consists mainly of a 'user input' section, where the user can edit experimental parameters and configure options relating to how the data will be processed, plotted, and saved.

Main control and auxiliary libraries

- mainControl.py: all experiments described in this protocol are run from the mainControl.py script, which takes an experiment-specific configuration file as an argument. Given the input parameters defined in the configuration file, mainControl.py runs the experiment, generates plots, and saves the results.
- DAQcontrol.py: contains functions that configure the DAQ unit
- SRScontrol.py: contains functions that control the SRS signal generator
- PBcontrol.py: contains functions that configure and program the PB card
- sequenceControl.py: contains functions that create the pulse sequences required to run the experiments in this protocol

Before running any experiments with qdSpectro, the user should read the readme file provided with the package, where any upgrades and patches will be described, and edit connectionConfig.py, as directed in this protocol.

To run an experiment with qdSpectro, do the following:

1 Open the relevant [variable text]config.py file in Notepad++. Read the description of the experimental parameters and data-processing options defined in this script.
2 Edit the experimental parameters and configure the data-processing options in the 'User Inputs' section of this script, as required. Save your changes.
3 To run the experiment, open a Windows command prompt and, from the working directory, run the following command:

```
python mainControl.py [variable text]config
```

4 To quit an experiment before it finishes running, press 'Ctrl' + 'c'.

A note on units: units for user-input parameters (entered in step 2 above) are specified in the comments accompanying the user-input section of the [variable text]config.py files. For added clarity, we also note here that the default unit for time variables in v.1.0.1 of the qdSpectro package (the current version at the time of writing) is nanoseconds. The user may either enter time variables in nanoseconds or use one of the following unit multipliers: `ns = 1, us = 1e3, ms = 1e6`. For example, if setting the variable `endTau` to 10 μs, the user may either enter `endTau = 10000` or `endTau = 10*us` in the user-input section of the relevant [variable text]config.py file. The latter format is used throughout the instructions given in this paper. For completeness, we also note that, in v.1.0.1 of qdSpectro, microwave frequencies are entered in hertz (e.g., if setting the variable `startFreq` to 2.7 GHz, the user should enter `startFreq=2.7e9`) and microwave powers in dBm (e.g., if setting the variable `microwavePower` to 0 dBm, the user should enter `microwavePower=0`). Users running a different version of qdSpectro should refer to that version's readme file for any version-specific user-input instructions.

The DAQ configuration used in this protocol and the APD signal connection instructions below assume that the APD input to the DAQ unit is a referenced single-ended (RSE) connection; if the user prefers to use a differential connection, the configureDAQ() function in the DAQcontrol.py script of qdSpectro must be edited accordingly.

29 Choose an AI terminal of the DAQ unit to which you will later connect the APD output voltage signal (note that the signal should be connected across the chosen AI terminal and the AI ground (AI GND) terminal of the DAQ unit). Set up the terminal to be connected via a BNC cable to the APD; depending on the choice of DAQ unit, this may require soldering a BNC connector to a short section of twisted-pair wires, which can be fed into the DAQ unit's screw terminals.

30 Connect two PB channels to two peripheral function interface (PFI) terminals of the DAQ unit, with ground terminals connected to the DAQ unit's digital ground (D GND). As in the previous step, depending on the choice of DAQ unit, this may require soldering a BNC connector to a short section of twisted-pair wires that can be fed into the DAQ unit's screw terminals. These two PB channels serve as the sources for the Sample Clock and the Start Trigger signals used by the DAQ unit to perform hardware-timed acquisition of the APD voltage signal input data (refer to the section of the DAQ unit manual on analog input timing signals, e.g., pages 4-11 to 4-22 in the NI USB-621x manual version from April 2009).

31 Open connectionConfig.py in Notepad++. Under 'DAQ connections', edit the definitions of the variables `DAQ_APDInput`, `DAQ_SampleClk`, and `DAQ_StartTrig` to match the names of the DAQ unit input terminals you have chosen for the APD voltage signal, PB-generated sample clock and start trigger, respectively (e.g., if the PB channel that will generate the start trigger is connected to terminal PFI5 on the DAQ unit, the relevant definition in connectionConfig.py should read `DAQ_StartTrig="PFI5"`). When defining the name of the AI channel connected to the APD,

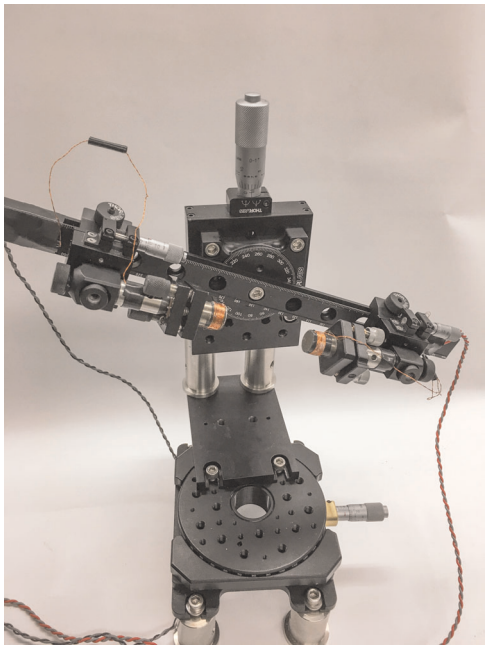

Fig. 10 | Magnet mount with *x*, *z* rotation for B_0 field alignment. Coils have been wound around the permanent magnets for small magnetic field adjustments, which are not described in the protocol.

Box 2 | Turning PB channels on and off

At several points throughout the setup of the apparatus described in this protocol, PB channels have to be toggled on and off (e.g., to test if the AOM is working and well aligned). Use the script togglePBchan.py to toggle any PB channel. In a Windows command prompt, start Python from the working directory and run `togglePBchan.py`. A key will be displayed relating a letter to a PB channel, as below:
- A = PB channel connected to the switch on the RF source driving the AOM.
- M = PB channel connected to the switch on the MW output of the SRS signal generator.
- I = PB channel connected to the switch on the I input of the SRS signal generator.
- Q = PB channel connected to the switch on the Q input of the SRS signal generator.
- D = PB channel connected to the DAQ unit's sample clock input.
- S = PB channel connected to the DAQ unit's start trigger input.

To turn on a given PB channel, type in the letter corresponding to it and press 'Enter'. To turn the channel off, type in the same key again and press 'Enter'. Check the functionality by measuring the PB output voltage on an oscilloscope.

it is useful to run the National Instruments Measurement and Automation Explorer (NI MAX) program to verify which device name has been assigned to the DAQ unit because the AI channel name will include this name (e.g., in v.17.0 of the NI MAX program, open the 'My System' drop-down menu and click to expand 'Devices and Interfaces'. Find your DAQ unit on the list: it will be labeled with a National Instruments model number (e.g., NI USB-6211) followed by the device name in quotes (e.g., 'Dev2'). If, for instance, the APD is connected to terminal ai1 and the DAQ unit has device name 'Dev2', the AI channel name that should be written into connectionConfig.py is 'Dev2/ai1'). Set `DAQ_MaxSamplingRate` to the maximum sampling rate of your National Instruments DAQ unit in samples per channel per second. Finally, set `minVoltage` and `maxVoltage` (in Volts) to match an AI voltage range that is supported by your DAQ unit and that accommodates the range of voltages output by your APD (e.g., the 'Analog Input' section of chapter 4 of the NI USB-621x manual version from April 2009 includes a table listing the supported input voltage ranges for the NI DAQ USB-621x series).

32 Also in connectionConfig.py, set the variable `PBclk` equal to the clock frequency of the PB card you are using, in MHz. Under 'PulseBlaster connections', edit the variable definitions for `PB_DAQ` and `PB_STARTtrig` to match the PB output bits that were chosen to output the sample clock and start trigger for the DAQ unit, respectively. For example, if you are using the SP18A ESR-PRO PB board and chose bit 2 (corresponding to the BNC2 connector on the board, as shown in Fig. 10 of the September/2017 version of the PulseBlasterESR-PRO manual) to output the start trigger pulses,

Box 3 | Connecting signals to the Mini-Circuits switch

The RF switch used in this protocol directs power applied to its RF input to one of its two RF outputs, depending on whether the signal at its TTL input is high or low (refer to datasheet for threshold high and low voltages). The version of the Mini-Circuits ZAWSA-2-50DR+ switch used in this protocol, for example, directs power to RF Output 2 when the TTL control is high and to RF Output 1 when the TTL control is low. We terminate RF Output 1 with a 50-Ω load and use the TTL control to switch on and off RF Output 2 (i.e., Output 2 is on when the TTL input is high and off when the TTL input is low). To avoid damaging the switch, the user should ensure that the unused RF output is terminated with a matched (50 Ω) load and that the switch is powered with the appropriate DC supply voltages before connecting an RF signal to the input port.

the relevant definition in connectionConfig.py should read `PB_STARTtrig =2`. Save your changes to connectionConfig.py. The user can check that the PB channel definitions are correct by monitoring the channels with an oscilloscope and running `togglePBchan.py` (a Python script that is part of the qdSpectro package), as described in Box 2.

! CAUTION Before proceeding, ensure that all staff who will be near the laser system or operating it have completed the appropriate laser safety training at your institution. In addition, the laboratory and the laser system itself must comply with the relevant institutional laser safety guidelines. Generally, researchers should follow the basic laser safety instructions, including wearing laser goggles, refraining from wearing reflective items and avoiding bringing your head to the laser height level.

! CAUTION Before proceeding, ensure that all staff who will be near the setup or operating it have completed appropriate MW and RF safety training at your institution. In particular, ensure that they are familiar with how to handle MW sources, amplifiers, and antennas safely.

33 *Mounting and alignment of the AOM (Steps 33–36).* Consult the AOM manual for the necessary RF input power of the AOM. Depending on the choice of AOM driver, there may be a number of options to enable switching the drive to the AOM. In general, the drive consists of an RF oscillator at the frequency required by the AOM (80 MHz, in our case) and an RF amplifier. We drive our AOM using a commercially available IntraAction AOM driver. Within the housing of the driver, there is an RF oscillator connected to an amplifier with an ordinary BNC cable. To achieve high extinction switching, we disconnected the oscillator from the amplifier, and inserted an MW switch between them, with the oscillator output connected to the switch input and the switch output (RF 2) connected to the amplifier input. Be careful to avoid unwanted grounding or shorting through these connections by properly isolating the components and cables. Terminate the second switch output (RF1) with a 50-Ω load (Box 3). Power the switch with +5V and −5V, provided by a power supply. Choose a PB channel to control the switch and connect the channel to the switch's TTL input. Update the definition of the variable `PB_AOM` in connectionConfig.py to match the output bit number of this PB channel. Before connecting the amplifier output to the AOM input, be sure you do not exceed the maximum RF input power specified in the AOM manual. First measure the drive power by connecting to an RF power meter and then adjust accordingly. Turn off the drive and connect to the AOM after power adjustment.

▲ CRITICAL STEP Depending on the AOM type, the procedure in Steps 33–35 will vary. Consult the manual for proper mounting and alignment. For a general overview, use Fig. 4 (optics) and 5 (electronics).

34 Install the 532-nm laser on an optical table. One possible arrangement of the optics of the experiment is depicted in Fig. 4. The beam waist must be no larger than the clear aperture of the AOM. To meet this condition, we demagnify the beam by a factor of 8, using a telescope consisting of a lens with a focal length of 400 mm and another with a focal length of 50 mm, separated by the sum of their focal lengths. The telescope preserves collimation of the beam before passing through the AOM. We choose to modulate the collimated beam in order to decouple divergence from diffraction by the AOM. Place a pedestal post holder (Thorlabs PH082E) with a 1-inch optical post (Thorlabs TR1) on a 5-axis aligner. Mount the AOM on the 1-inch optical post. We recommend attaching a heat sink to the AOM for efficient heat dissipation. Place the 5-axis stage with the AOM in the laser path a few centimeters in front of the 50-mm focal-length lens. Turn on the laser and attenuate to <1 mW for alignment. Turn on the PB channel controlling the AOM switch, using the togglePBchan.py script as described in Box 2. Adjust the height and the position of the AOM such that the laser beam passes through the center of the device's aperture. Observe the laser spot on a piece of paper or cardboard placed after the AOM. Laser goggles may help with visualization at this

point because they block the intense laser light and pass the faint luminescence of the paper or cardboard. Turn on the AOM driver. When the AOM is turned on and is nearly aligned, both a zeroth and first-diffraction-order spot should be visible. Use an iris to pass the first diffraction order and to block the zeroth diffraction order. Measure the optical power of the first diffraction order after the iris with a power meter. Maximize the power shunted into the first diffraction order by adjusting the degrees of freedom of the 5-axis aligner. Carefully adjusting the RF power of the AOM driver can also improve diffraction efficiency; however, if the RF power is set too high, several diffraction orders become visible and the AOM might be damaged. Once optimized, measure the ratio of RF power in the first and zeroth diffraction orders. Compare with the diffraction efficiency quoted in the AOM manual.

▲ **CRITICAL STEP** Check the extinction ratio, i.e., the ratio of laser power in the first-order beam with the AOM switched on and off. A high extinction ratio is necessary to avoid unwanted repolarization of the NVs when the AOM is nominally off. This number should be 8,000–10,000. If this is not the case, the extinction ratio can be improved in the next step.

35 To improve the extinction ratio, we focus the first diffraction order with a lens of focal length 100 mm placed after the iris. At the focal plane of this lens, we place a 200-μm pinhole mounted on a translating lens mount for fine lateral adjustment. Re-collimate the beam after the pinhole. We use a lens of focal length 200 mm placed a focal distance after the pinhole.

36 Place a $\lambda/2$ waveplate in a continuous-rotation mount between the pinhole and the 200-mm focal length lens (Fig. 4). Exact placement of the waveplate in the laser path after the AOM is not important.

37 *Mounting of magnets on an* xy*-translation stage with a rotating platform (Steps 37–39).* Install an *xy*-translation stage with a rotating platform with four 1.5-inch pedestal pillar posts (Thorlabs RS1.5P) on the laser table. These define the position of the APD and the center of the NV experiment. Consult Fig. 4 for an overview of the entire experiment and the relative positions on the laser table. Place a 1-inch pedestal post holder (Thorlabs PH082E) beneath the stage, centered at its rotational axis.

38 Mount two 3-inch pedestal pillar posts (Thorlabs RS3P) on the same short edge and on the top side of a mounting base. Install a right-angle bracket with a 1 inch translation stage on top of the pedestal pillar holders. The micrometer screw of the translation stage should point up. Mount a 2-inch-diameter manual rotation stage on the upper part of the 1 inch translational stage. Mount the assembled piece on the *xy*-translation stage with a rotating platform, using the screw holes at the outer edge. The central part of the rotating platform should be kept free for the APD, which will be mounted later.

39 Install two dovetail rail carriers on the dovetail optical rail and place them 3–4 inches apart. On each rail carrier, mount a 1/4-inch travel single-axis translation stage that carries a 0.75-inch aluminum post (Thorlabs TRA075). The translation axis must be parallel to the optical rail. Use instant adhesive to glue two permanent magnets to the centers of two compact kinematic mirror mounts.

▲ **CRITICAL STEP** Ensure that one magnet is glued down on its north pole, and the other one on its south pole. When the magnets are properly oriented, they tend to pull toward each other. Mount each of these mirror mounts to the 0.75-inch posts via a 1-inch post (Thorlabs TRA1) and a right-angle end clamp. The magnets should face each other and should be aligned parallel to the rail carrier. Install the assembled rail on the center of the 2-inch diameter rotation stage (Fig. 10).

40 *Assembly of the excitation and detection components (Steps 40–46).* Mount two fixed 90° brackets with two 2-inch mini-series mounting posts (Thorlabs MS2R) on the threaded holes at the top of the large-area APD. The posts should be parallel to the edge and to the top side of the APD, as well as to one another. The posts are used to mount the APD and to affix the light guide and fluorescence filter to the APD. Screw the two 1-inch mini-series mounting posts into the two 90° brackets. Mount each of these onto the mini-posts on the APD such that the 1-inch mini-posts point perpendicularly to the face of the APD. Place them so that they are on different 2-inch mini-posts and on different corners of the APD. Screw in an adaptor with external SM1 threads and internal SM05 threads into a removable cage plate so that it is flush with the magnetic face. Screw a lens tube into the adaptor plate on the opposite site of the magnetic face. Use two rings to mount the fluorescence filter (e.g., Semrock BLP01-647R) toward the end of the lens tube. Mount the assembled filter holder on the mini-posts of the APD (Fig. 11). The fluorescence filter should sit directly on the APD.

41 Use an 8-32 set screw to combine 1- and 1.5-inch-long optical posts into an effective 2.5-inch post. Mount this elongated post to the center of a mounting base. The post will be inserted into the

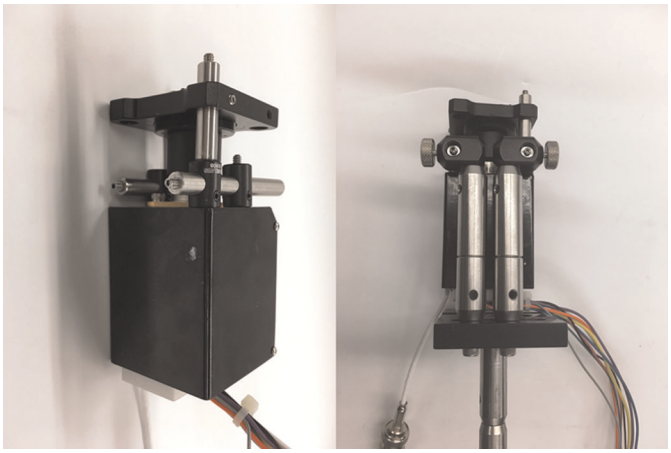

Fig. 11 | Avalanche photodiode (APD) holder. Left, side view. Right, rear view.

pedestal post holder centered beneath the rotating platform (Step 37). Use 1/4-inch 20 set screws to make two additional effective 2.5-inch posts by combining the remaining 1- and 1.5-inch posts. Mount these optical posts on the top of the mounting base, within the same slot. Separate the swivel post clamp into two parts. Remove the thumb screw from the end that has the counterbore hole. Mount both post clamp parts on the 2.5-inch posts. The through holes should be parallel to the long edge of the base and the thumb screws should point outward. Adjust the spacing of the 2.5-inch posts in order to slide the 2-inch mini-series posts on the APD into the post clamps. Place the assembled APD mount into the pedestal post holder centered beneath the rotating platform (Step 37). Keep some distance between the base plate and the rotational stage so that it can be freely moved.

42 Use optical epoxy to glue the diamond centered on the top of the light guide (e.g., 50-mm-long hexagonal light pipe with 4-mm aperture; the diameter depends on the diamond size).
▲ **CRITICAL STEP** Keep the amount of glue as small as possible and ensure that the NV layer is facing up (see also Step 45). Remove one of the retaining rings of the light guide mount (e.g., 4 mm × 25-mm light pipe) and place it on the light pipe. Place the retaining ring with the light pipe in a SM1-threaded adaptor with smooth internal bore (16-mm diameter) and use its screws to tighten the light guide. Screw the threaded adaptor into the front part of the removable cage plate and place it on its magnetic counterpart on the APD. Push the light guide down until it is in contact with the fluorescence filter.
▲ **CRITICAL STEP** Do not scratch the filter.

43 Mount a heat sink at the metallic side of the APD. Use thermal paste to improve thermal contact.
! **CAUTION** Consult the safety data sheet of the thermal paste for handling. The heat sink should in turn be cooled by a small fan. Consult the APD manual for details about powering: power the APD with +12, −12V, and GND from a power supply. The onboard cooling of the APD must be connected to +5V and GND.

44 Place two mirrors into the laser path after the pinhole (Fig. 4). They are used to direct and to align the laser beam onto the diamond (Fig. 4 inset). Use a third mirror and flip it 90° with angle clamps (and a 1-inch post) to direct the laser beam away from the optical table and toward the diamond (Fig. 4). Ensure that the laser is at low power (<1 mW) for alignment and turn on the AOM to pass the laser toward the diamond. The laser can be directed into the diamond either directly through a polished side of the diamond or first through a face of the light guide (Fig. 4) and into the bottom face of the diamond. In either case, the angle of incidence must be chosen to ensure total internal reflection at the diamond–sample interface. Use a lens (e.g., 30 mm) to focus the laser onto the diamond. The focal length depends on the laser beam diameter and the desired laser spot size at the NV layer (in our case, we design for an ~30-μm-diameter beam waist at focus). To position the laser spot on the diamond, place the lens in a lens mount attached to posts (two 1-inch aluminum posts (Thorlabs TRA1)) screwed at the other end into a 1/2-inch *xyz* dovetail translation stage with baseplate. Orient the lens in a way such that one translation axis of the stage is parallel to the lens axis. This degree of freedom is used to adjust the position of the focal spot on the diamond. Anchor the translation stage to the optical table by mounting it with a right-angle clamp and a sufficient number of posts (Fig. 12). The distance of the lens to the diamond should be roughly equal to the focal length.

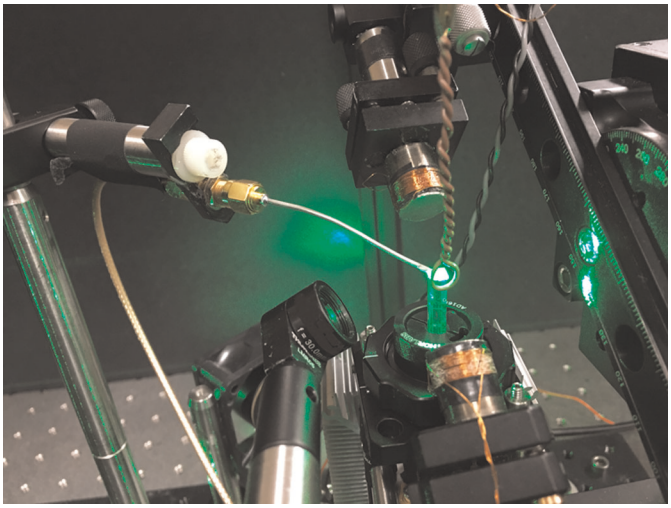

Fig. 12 | Photo of the quantum diamond spectrometer. On the right, the magnet mount is shown (coils have been wound around the static magnets for small magnetic field adjustments, which are not described in the protocol). In the center of the magnets is the light guide with the diamond (bright green because of illumination). From the top, an RF loop is positioned near the diamond for sensing a generated signal. At the center bottom, the 30-mm lens for focusing the laser beam can be seen. The mount for the microwave delivery loop is located at top left of the picture.

45 To fine-tune the laser spot alignment, first check that the portion of the laser beam reflected from the top surface of the diamond leaves the apparatus at an angle similar to that of the incoming laser beam. Second, move the laser spot onto the NV region of the diamond. With laser safety goggles on, turn up the laser power to see a red spot on the diamond caused by the NV fluorescence. We typically use ~50–100 mW of continuous-wave laser power after L4. Adjust the focusing lens to minimize the laser spot size at the NV layer position. Usually two weak red spots and one bright spot are observable. The two weak spots are caused by light going through the light guide–glue–diamond interface. If you observe two bright spots on the bottom of the diamond, the diamond is mounted incorrectly, with the NV layer pointing down. In this case, use acetone to dissolve the glue and remove the diamond from the light guide. Then, acid-clean the diamond as described in Steps 1–11 and glue it with the NV layer up.

? TROUBLESHOOTING

46 Power the APD. Make sure that the APD is cooled by a fan. Check to see that the APD responds to the fluorescent light by monitoring the output voltage on an oscilloscope. You should see a voltage change upon switching the AOM on and off. Connect the APD output to the DAQ AI channel you selected in Step 29. We typically measure a photovoltage in the range of 100–400 mV (approximately few hundred nanowatts) on our DAQ unit.

47 *Construction of loop for MW delivery (Step 47).* Cut off a 5-cm piece of the semi-rigid coaxial wire. Use a wire stripper to remove ~3 mm of the outer part of the coaxial wire and the dielectric material so that the inner wire is free. Place the white isolation ring of the SMA straight solder plug on that wire (Fig. 13). Plug the golden pin into the white dielectric cylinder. Solder the inner wire to the golden pin. The white isolation ring and cylinder should be in contact. Place the coaxial wire connected to the pin into the SMA connector. The pin should point into the threaded part of the connector. On the opposite side, use solder to fill up the gap between the coaxial wire and the SMA connector for a conductive connection of the ground. Use a wire stripper to remove ~3 mm of the outer part at the end of the coaxial wire and the dielectric material so that the central wire is free. Bend it over to form a loop. Solder the end of the interior wire to the outer part of the coaxial wire.

▲ CRITICAL STEP The loop size depends on the needs of MW field strength and homogeneity. A smaller loop generates higher MW fields with higher spatial gradients; a bigger loop has the opposite effect.

48 *Setup of signal source (Steps 48 and 49).* Connect the GPIB port of the MW signal source (SRS signal generator) to a USB port on the PC, using the GPIB/USB converter. Enable the GPIB interface on the SRS signal generator and select its GPIB address by following the GPIB setup instructions in the SRS manual (e.g., for models in the SG380 series, see page 46 of the SG380 series manual Revision 2.04). In the 'SRS connections' section of connectionConfig.py, set the variables `GPIBaddr` and `modelName` to be the GPIB address and model name of the SRS (e.g., `GPIBaddr=27`, `modelName='SG384'`).

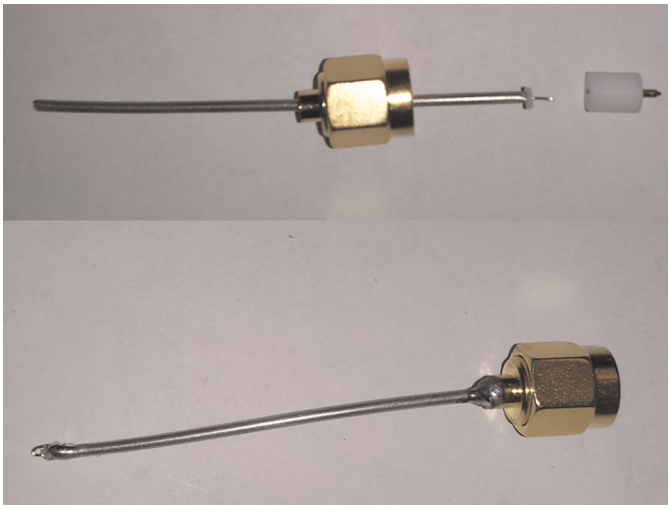

Fig. 13 | Microwave delivery loop. Top: individual parts of the MW delivery loop before assembly. Bottom: assembled MW loop.

! CAUTION Turn off the RF output of the SRS before continuing. If using the SRS SG384 model, this is done by pressing the 'Shift' button, followed by the 'AMPL' button on the SRS. The SRS screen will display 'N-type OFF' when this is done, to indicate that the RF output of the SRS is off. Scripts in the qdSpectro package will instruct the PC to send remote commands to turn on the SRS RF output during the experiments, but this output should be kept off while the MW path is being built. Install one MW switch and power it with +/−5 V from a power supply (Fig. 5). Connect the RF output of the SRS signal generator (the N-type output for the SG384 model) to the RF input of the switch, using the N-SMA adaptor and an SMA cable (Box 3). Choose a PB channel to control this switch and connect the channel to the switch's TTL input. Update the definition of the variable `PB_MW` in connectionConfig.py accordingly. Connect RF Output 2 of the switch to the input of the MW amplifier and terminate RF Output 1 with a 50-Ω load. Use a circulator to protect the output of the amplifier from potentially damaging MW reflections.

! CAUTION Make sure that you connect the circulator to the amplifier with the correct polarity. Connect the circulator on the amplifier to the MW loop with an SMA cable and SMA female-SMA female adaptor. Use the SMA female–female adaptor to mount the loop with a clamp to two posts connected to the table with a right-angle clamp. Adjust the height of the mount and bend the coaxial wire so that the loop is in contact with the diamond and the laser spot is centered in the loop (Fig. 13).

! CAUTION Consult the amplifier manual for handling instructions. Do not exceed maximum input power. Ensure that the amplifier is on (i.e., supplied with its required DC voltages) before feeding RF signals into its input port. General guidelines for turning on and off amplifiers are given in Box 4, but safety guidelines outlined in your amplifier's manual or provided by the manufacturer take precedence and must be read and followed.

49 Set up the IQ phase control: for the nuclear spin–sensing experiments, the phase of the MW pulses must be controlled, which we achieve by use of the internal IQ mixer of the SRS signal generator SG384. For a detailed description of the IQ mixer and its calibration, consult the manual. To control the four phases ($x = 0°$, $-x = 180°$, $y = 90°$, $-y = 270°$, see also Table 1), the SG384 needs two inputs through which each can be switched between $\pm 0.5/\sqrt{2}$ ~0.35 V. Use a stable power supply with +0.35 V and −0.35 V and split it with a T connector at each output. Install two MW switches. Connect +0.35 V to RF Output 1 and −0.35 V to RF Output 2 of each of the two MW switches.

▲ CRITICAL STEP Ensure that the absolute value is 0.35 V in both cases. Connect the input of the switches to the IQ inputs of the SG384. Power the switches with ±5 V. Connect the TTL inputs of the switches to two PB channels and update the definitions of the variables `PB_I` and `PB_Q` in connectionConfig.py accordingly.

NV diamond characterization experiments ● Timing 2 weeks

50 *Finding the NV-ESR transition at ambient magnetic field (Step 50).* Remove the magnets to work at near-zero applied magnetic field (i.e., at the Earth's field). This makes it easier to find the NV-ESR

Box 4 | Amplifier turn-on and turn-off orders

When testing and operating MW and RF amplifiers, the user must read and follow all amplifier safety guidelines given by the manufacturer of the amplifier. Some general good-practice guidelines are given below, but these do not replace manufacturer safety guidelines and should be followed only if they do not contradict manufacturer instructions/guidelines, which always take precedence. In general, amplifier turn-on and turn-off order is as described below.

Amplifier turn-on order

1 Terminate the amplifier, either with a matched load or with the load with which it will be operated (e.g., antenna loop). If the load is not matched, as is the case with the loop antenna we use in this protocol, it is good practice to place a circulator or isolator directly after the amplifier to prevent the formation of standing waves. Ensure that the isolator/circulator is connected in the correct direction and can handle signals at the power and frequency range output from your amplifier.
2 Once the amplifier is terminated, turn on its voltage supply to power it with the required DC voltages.
3 Last, connect the MW source to the input of the amplifier and turn the source on, ensuring that you do not exceed the rated input power of the amplifier.

Amplifier turn-off order

1 Turn off the MW source.
2 Turn off the amplifier's DC power supply.
3 You may now disconnect the load from the output of the amplifier.

resonance for the first time. Refer to Box 1 for a description of the qdSpectro package and how to run experiments. Open ESRconfig.py in Notepad++, read the description of the variables and data-processing options defined in this script and change the frequency sweep values to 2.7–3.0 GHz with a step size of, e.g., 3 MHz (i.e., set `startFreq=2.7e9`, `endFreq=3e9`, and `N_scanPts=101`). Set the `microwavePower` variable, which sets the output power level of the SRS signal generator in dBm to a level that is below your amplifier's maximum input, e.g., we set `microwavePower=0` (units are dBm) when using the Mini-Circuits ZHL-16W-43+ amplifier. The duration of the pulse sequence (the signal-acquisition half), `t_duration`, should be set to 80 μs, with 10,000 samples taken per scan point (i.e., set `t_duration=80*us` and `Nsamples=10000` in `ESRconfig.py`). Turn on the MW amplifier. Run `python mainControl.py ESRconfig`. Check the pulse sequence by monitoring all the PB output channels on an oscilloscope and comparing them with the pulse sequence shown in Fig. 6. Two dips should be visible in the data (Fig. 6a). The contrast may vary depending on MW power, pulse sequence duration, and properties of the diamond.

? TROUBLESHOOTING

51 *Running NV-ESR: alignment and adjusting magnetic field (Step 51).* Turn off the AOM, using `togglePBchan.py` (Box 2). Mount the magnets at the ends of the rail so that each magnet is roughly equidistant from the laser spot on the diamond. Also use *x* and *y* of the rotational stage to move the magnets so that the diamond and the laser spot are centered between the two magnets. Rotate the stage so that the magnet faces are parallel/perpendicular to the edges of the diamond (if the diamond is cut perpendicular to [110] facets) and tilt the rail ~36° out of the horizontal plane. This gives a rough alignment of the B_0 field along one of the NV axes. Turn on the AOM and run `python mainControl.py ESRconfig`. Depending on the magnetic field strength, sweep the MW frequency between 1.8 GHz and 4 GHz in 3-MHz steps. If the experiment is not aligned along one of the four possible NV axes (which is very likely, see Fig. 14), up to 8 NV-ESR transitions will appear in the NV-ESR spectrum (excluding additional splittings due to hyperfine interactions).

▲CRITICAL STEP Importantly, transitions due to different NV orientations may have unequal amplitudes in their resonance lines, and weak transitions can be easily missed. To tune transition rates (and thus resonance line amplitudes), adjust the laser polarization by rotating the $\lambda/2$ waveplate, adjust the MW polarization by moving the loop (however, this is not recommended once high contrast has been achieved), or increase the MW power (without exceeding the maximum input power of your amplifier). Keep in mind that high MW power induces power broadening.

▲CRITICAL STEP For the quantum sensing protocol, the B_0 field must be aligned along one NV axis. The three inner transitions then overlap (they all see the same projection of B_0), and only four resonance lines (without hyperfine lines) appear, two on each side of the zero-field splitting (Fig. 14). Try to overlap the resonances of the off-axis NV orientations by using the two rotational degrees of freedom of the magnetic mount. One can also use the mirror holders on which the magnets are glued for fine tuning. If all of these lines overlap within their linewidths, the misalignment is typically smaller than a few degrees. After successfully aligning the experiment, tighten the set screws of the

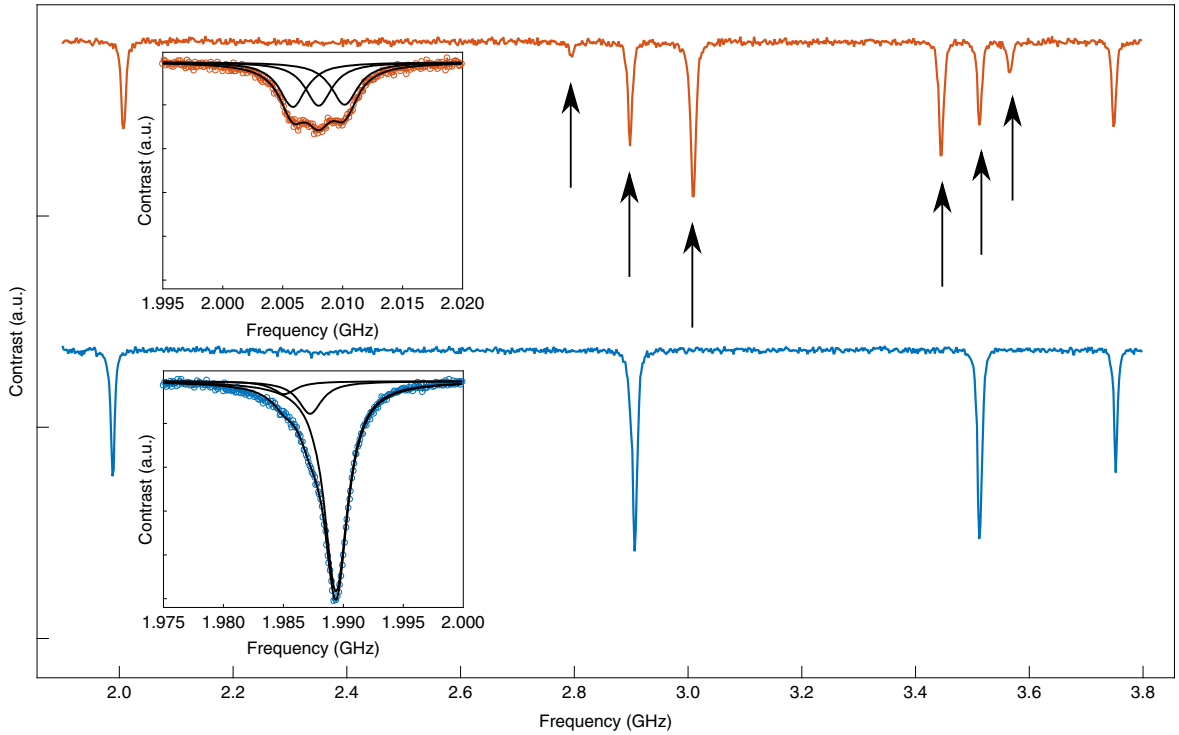

Fig. 14 | Magnetic field alignment. Top: Magnetic field is not aligned along an NV axis. All 2 × 4 NV-ESR transitions can be observed. The arrow-marked resonances must overlap for alignment. The inset shows that the three hyperfine transitions have equal amplitudes in the misaligned case. Bottom: Magnetic field is aligned along one NV axis. In this case, the magnetic field projection on the other three NV axes is identical and the resonances overlap. Now the hyperfine pattern is polarized as shown in the figure inset.

rotational stages. Now use the slider on the rail to adjust the magnetic field strength. The magnetic field strength can be calculated from the observed Zeeman shift according to Eq. 6. For example, if one would like to work at 310 G, then move the lowest NV resonance to ~2 GHz.

▲ **CRITICAL STEP** Always try to keep the diamond centered between the magnets. If it is not in the center, magnetic field gradients might lead to unwanted line broadening. To check this, reduce the MW power to reduce power broadening and increase the number of samples or averages to improve the SNR. Look at the resonance with the lowest (or highest) transition frequency, which corresponds to NVs aligned along B_0. If hyperfine splitting caused by the ^{14}N nuclear spin can be observed, then the gradient is <1 G over the laser spot, which is sufficient for the following experiments (Fig. 14, inset). You can also use the hyperfine amplitudes as an alignment diagnostic if you work at moderate fields (in the range 250–1,000 G). In the case of poor alignment, the three hyperfine lines exhibit similar amplitudes. In the aligned case, the ^{14}N nucleus is polarized[57,58] as can be seen in Fig. 14.

? TROUBLESHOOTING

52 *Running NV-ESR: determining ESR resonance frequency and B_0 field strength (Step 52).* Open ESRconfig.py in Notepad++ and change frequency sweep values around the expected resonance frequency after alignment. Typically, we drive the lowest resonance frequency ($m_s = 0$ to $m_s = -1$). Run `python mainControl.py ESRconfig`. Use the center frequency of the dip to calculate B_0 according to Eq. 6.

53 *Setting the timing between the readout pulses (Step 53).* Although the PB outputs the AOM and DAQ unit trigger pulse in synchrony, these pulses usually do not coincide in real time because of a finite AOM response time and cable length differences. Open optimReadoutDelay.py in Notepad++. This script sweeps the readout delay between the start of the AOM and the DAQ unit pulse. Edit the `startDelay` and `endDelay` variables to set the sweep range of the delay, e.g., we use `startDelay = 10*ns` (note that the `startDelay` must be at least `5*t_min`, where `t_min` is the time resolution of the PB, which, for a 500-MHz-clock board, is 2 ns), `endDelay = 10000*ns`, with 100 points in the sweep (set by `N_scanPts`). Run `python optimReadoutDelay.py`. The recorded data show temporal overlap of these pulses (Fig. 15). The photovoltage is zero if there is no overlap and increases if both pulses overlap.

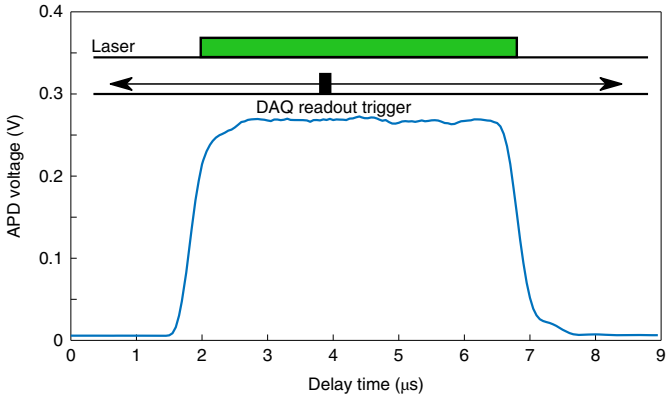

Fig. 15 | Setting timing between the readout pulses. DAQ unit readout pulse (small black box) is moved in time relative to the AOM pulse (green box). The data show the temporal overlap and the optimal timing when the maximum photovoltage is reached (at ~2.0 μs in our case).

▲ **CRITICAL STEP** The optimum readout time is sufficiently late in the photovoltage rise (i.e., at ~2 μs in Fig. 15). Enter this delay as the value of the variable `t_readoutDelay` in the config files of all experiments that follow in this protocol (i.e., Rabiconfig.py, T2config.py, XY8config.py, correlSpecconfig.py, T1config.py). This setting will remain fixed as long as there are no physical changes to the setup (e.g., changes to AOM alignment or cable lengths).

54 *Optimizing Rabi contrast (Steps 54 and 55).* Open Rabiconfig.py in Notepad++. Set the `microwaveFrequency` variable to the resonance frequency of the NV (Step 52) and set `microwavePower` to ~10 dB below the amplifier's maximum input power. Set `t_readoutDelay` as determined in Step 53. Run `python mainControl.py Rabiconfig`. Rabi oscillations should be observed in the data (Figs. 6b and 16). The frequency of the oscillation can be adjusted by changing the MW power.

▲ **CRITICAL STEP** Sensitivity to NMR signals in later steps improves linearly with the contrast (amplitude) of the Rabi oscillation observed here. The contrast should be optimized each time you change diamond, diamond orientation, and/or sample.

? TROUBLESHOOTING

55 Optimize the contrast by changing the laser polarization by rotating the $\lambda/2$ waveplate and by ensuring efficient NV repolarization. During an AOM pulse, the NVs must be reset to their $m_s = 0$ state. If NVs are not repolarized efficiently, the contrast will decrease. In our work, we find that efficient repolarization is achieved by using 100–200 mW of laser power in an ~(30 μm)^2 laser spot with an AOM pulse duration of 5 μs. One can change any of these three parameters in order to improve the repolarization. Improve SNR by increasing the number of samples and averages as needed to visualize the signal and reference data of the Rabi experiment (Fig. 16). If efficient NV repolarization is achieved, the Rabi oscillation will be observed only in the signal channel. If the NVs are not repolarized efficiently, the oscillation will also appear in the reference channel. The simplest way to optimize NV repolarization is to decrease the laser spot size by translating the focusing lens. If there is insufficient SNR to see the Rabi oscillation in the signal channel, optimize the contrast by adjusting the laser spot size and power, as well as the AOM pulse duration. Importantly, if the laser intensity is too high, the contrast will again be diminished because repolarization occurs faster than the readout time of the DAQ unit.

? TROUBLESHOOTING

56 *Running Rabi: determining the π and π/2 pulse durations.* Run `python mainControl.py Rabiconfig` with the previously presented parameters.

▲ **CRITICAL STEP** Note the MW pulse duration at which the first signal minimum occurs; this is the π-pulse duration (Fig. 6b). To change the Rabi frequency, adjust the power of the MW and/or the position of the laser spot with respect to the MW loop wire. With this experimental setup, we find that π-pulse durations of 20–60 ns are achievable.

? TROUBLESHOOTING

57 *Running an NV Hahn-echo experiment: determine NV-T2 relaxation time.* Open T2config.py in Notepad++. Set the MW frequency (`microwaveFrequency`) to the resonance frequency of the NV. Set the MW power (`microwavePower`) and the π-pulse duration (`t_pi`) to the values obtained in the Rabi experiment (Step 56). The minimum sweep time τ (`startTau`) should be longer than the π-pulse duration (e.g., for `t_pi =24*ns`, set `startTau=100*ns`). Conclude the

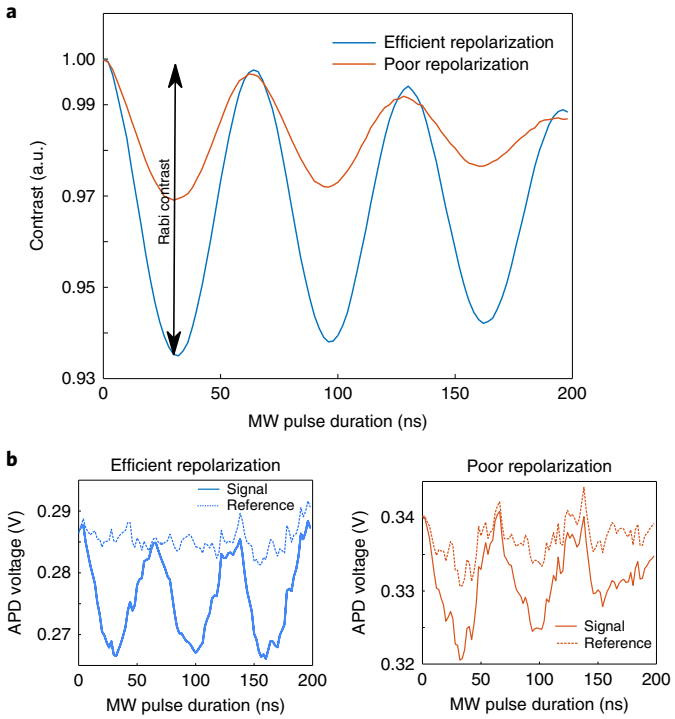

Fig. 16 | Rabi contrast. a, Rabi data show efficient and poor repolarization of the NVs. Poor repolarization results in a decrease in contrast. **b**, Raw data shown for these two cases. Left: in the case of efficient repolarization, the reference channel does not show Rabi oscillation. Right: in the case of poor repolarization, the NVs have not been reset and the Rabi oscillation also occurs in the reference. To acquire the poor repolarization data, we increased the laser beam size.

sweep at `endTau=10*us` (depending on the NV-T2 relaxation time). Set `t_readoutDelay` as determined in Step 53. The IQ function of the SRS signal generator must be activated. Set `numberOfPiPulses=1` to produce a Hahn-echo sequence consisting of a single π-pulse sandwiched between two $\pi/2$ pulses, with τ defined as the delay between the $\pi/2$ and π pulses, as shown in Fig. 6c (if one sets `numberOfPiPulses>1` to produce a sequence with multiple π pulses, qdSpectro will instead interpret τ as the delay between the π pulses, as explained in the user-input comments in T2config.py). Run `python mainControl.py T2config`. The acquired data should show a decay, as in Fig. 6c. The contrast at short times should be slightly less than half of the contrast in the Rabi experiment. For long τ, the contrast must go to zero. If this is not the case, it indicates that either the $\pi/2$ and π-pulse durations are not correct, or the IQ mixer is not working properly.

? TROUBLESHOOTING

58 *Running an NV-T1 experiment: determine NV-T1 relaxation time.* Open T1config.py. Change the MW frequency (`microwaveFrequency`) to the resonance frequency of the NV. Set the MW power (`microwavePower`) and the π-pulse duration (`t_pi`) to the values obtained in the Rabi experiment (Step 56). Set `t_readoutDelay` as determined in Step 53. Set the sweep range to 0–5 ms and use 1,000 samples (i.e., set `start_t=0*ms`, `end_t=5*ms`, `Nsamples=1000`. Note that, if `start_t` is set to 0 or to any value smaller than `(t_readoutDelay + 2*t_min*round(1*us/t_min) + t_pi)`, qdSpectro will automatically shift it by `(t_readoutDelay + 2*t_min*round(1*us/t_min) + t_pi)` to avoid pulse overlap errors, as detailed in the documentation under the user-input section of T1config.py). Keep in mind that NV-T1 experiments might take a long time. Run `python mainControl.py T1config`. The acquired data should show a decay, as in Fig. 6f.

Quantum sensing procedure for the detection of nuclear and electronic spins

▲ CRITICAL We recommend sensing an external AC signal as described in Box 5 and Fig. 17 before NMR signal detection to check the functionality of the experiment.

59 For running an XY8-*N* dynamic decoupling sequence for surface NMR signal detection, follow option A. For running correlation spectroscopy for surface NMR signal detection, follow option B. For running NV-T1 experiments for surface electronic spin detection, follow option C.

Box 5 | Detecting external AC magnetic fields with XY8-*N* sequence for calibration

It is often useful to sense synthetic signals generated by an RF loop, e.g., to calibrate the experiment and/or for troubleshooting if nuclear spin signals cannot be observed. Use the following procedure to check that the XY8-*N* pulse sequence is working correctly:

1. Determine the NV resonance frequency according to Step 52.
2. Repeat the Rabi experiment (Step 56) to determine the $\pi/2$ and π durations.
3. Open XY8config.py in Notepad++. Set the MW frequency to the resonance frequency of the NV. Set the MW power and the π-pulse duration to the values obtained in the Rabi experiment. The starting value of the swept time should be longer than the π-pulse duration (e.g., for `t_pi=24*ns`, we use `startTau=280*ns`) and conclude the sweep at ~500 ns. Use maximum allowed sampling rate (i.e., 4 ns). Use $N = 1$ to begin with. Set `t_readoutDelay` as determined in Step 53. Run `python mainControl.py XY8config`. One should see a decay, as shown in Figs. 6d and 17.
4. Place a wire loop next to the diamond (e.g., see RF loop in Fig. 13) and connect it to a signal source (e.g., the Rigol DS1022). If possible, try to mount the loop so that its magnetic field points along the B_0 direction. Turn on the signal source, set the frequency to, e.g., 1.25 MHz and use a safe output power level.
5. Run `python mainControl.py XY8config`. Sweep `τ` from 280 ns to 500 ns. Use the MW frequency and power, as well as the π-pulse duration determined in the previous NV-ESR and Rabi experiment. It is easier to see the signal for higher *N*, e.g., in our case $N = 12$. A 1.25-MHz frequency signal should give a dip at 400 ns [=1/(2 × 1.25 MHz)] in the XY8-*N* decay curve (Fig. 17). This indicates that the pulse sequence works as expected. *N* should be optimized by comparing the SNR for the same total duration of the experiment.

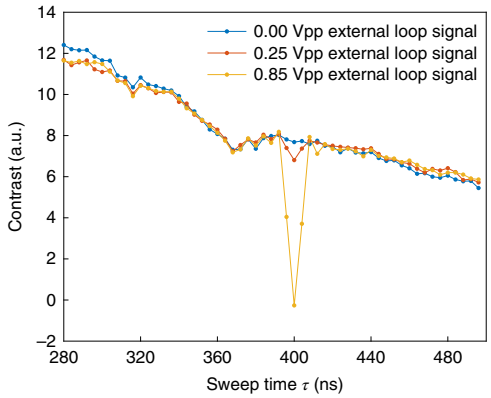

Fig. 17 | Detection of an external AC signal from an RF loop at 1.25 MHz with an XY8-12 dynamic decoupling sequence. Keep in mind that the depicted voltages are relative values and depend on, for example, the loop design, orientation and distance to the diamond. Vpp, peak-to-peak voltage.

(A) **Running an XY8-*N* dynamic decoupling sequence for surface NMR signal detection** ● **Timing 2 h**

(i) Pipette a droplet of the NMR sample onto the diamond's surface at the laser spot. Keep in mind that the refractive index of the sample might change the total internal reflection condition, which in turn may lead to reduced Rabi contrast. When performing this step for the first time, we recommend cleaning the diamond with IPA. Protons can usually be sensed even on a 'clean' diamond surface, probably due to the presence of a nanoscale hydrocarbon film on the surface. Other useful samples for initial experiments are PDMS (for ^{1}H) or Fomblin oil (for ^{19}F), as shown in Fig. 18.

(ii) Determine the B_0 field with the NV-ESR procedure according to Step 52 and Eq. 6. Calculate the nuclear spin resonance frequency f_L by multiplying the B_0 field strength in gauss by the gyromagnetic ratio in megahertz per gauss (Eq. 5). Calculate $\tau_0 = 1/(2f_L)$, to be set as the time spacing between π pulses in the XY8-*N* sequence. Reasonable τ_0 values are between 300 and 2,000 ns.

(iii) Repeat the Rabi experiment (Step 56) to determine the $\pi/2$ and π-pulse durations. In some cases, the Rabi contrast decreases upon placing a sample on the surface because of background fluorescence of the sample or because the total internal reflection condition is no longer met. Note that the sample can also influence MW delivery.

(iv) Open XY8config.py in Notepad++. Set the π-pulse duration (`t_pi`) and MW frequency (`microwaveFrequency`) according to the previous steps. Sweep τ around τ_0 with, for example, 50 points and 4-ns spacing, which is double the smallest step size (`t_min`) allowed by our PB card (recall, as shown in Fig. 6d, that τ in the XY8 sequence is defined as the delay

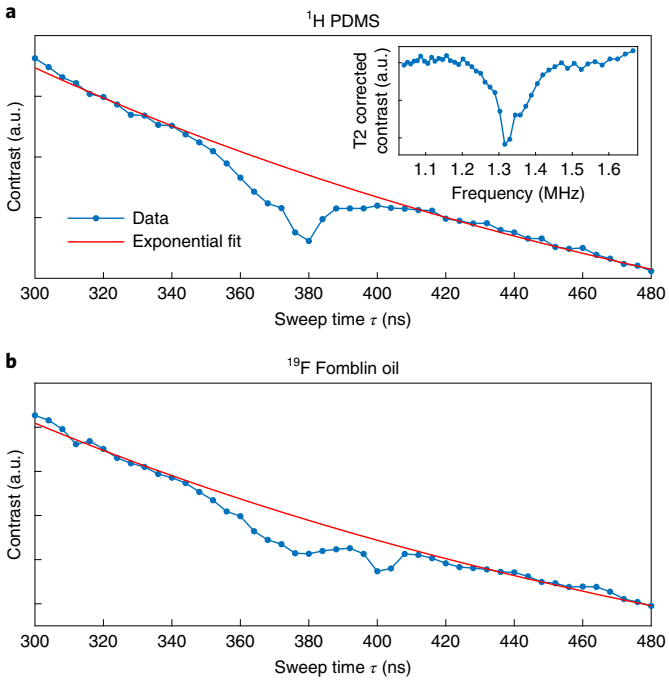

Fig. 18 | Nuclear spin sensing with a dynamic decoupling sequence at 311 G. a, ^{1}H NMR detection of PDMS on the diamond surface. The red line is a mono-exponential fit of the NV-T2 decay. Inset: decay-subtracted data plotted on a frequency axis. **b**, ^{19}F NMR detection in Fomblin oil. The broad feature ~378 ns is due to background protons. The red line is a mono-exponential fit of the NV-T2 decay. In both cases, 40-ns π pulses, 10,000 samples, 20 averages, 4-ns sampling intervals, and $N = 12$ were used.

between successive π pulses, which is double the delay between the $\pi/2$ pulses and π pulses. Because the timing resolution of our 500-MHz PB card is 2 ns, τ must be stepped by at least 4 ns in this pulse sequence. If using a different PB card, set the spacing to `2*t_min`. Depending on the diamond, one should use $N > 8$, 10,000 samples, and 5–10 averages (by setting the variables `N`, `Nsamples` and `Navg`, respectively). Set `t_readoutDelay` as determined in Step 53. N should be optimized by comparing the SNR for the same total duration of the experiment.

(v) Run `python mainControl.py XY8config`. The acquired data should resemble those in Fig. 18.

? TROUBLESHOOTING

(B) **Running correlation spectroscopy for surface NMR signal detection** ● **Timing 2 h**

(i) Pipette a droplet of the sample onto the diamond's surface at the laser spot. Keep in mind that the refractive index of the sample might change the total internal reflection condition, which in turn may lead to reduced Rabi contrast. When performing this step for the first time, we recommend cleaning the diamond with IPA. Protons can usually be sensed on a 'clean' diamond surface, probably because of the presence of a nanoscale hydrocarbon film on the surface. Other useful samples for initial experiments are PDMS (for ^{1}H) or Fomblin oil (for ^{19}F), as shown in Fig. 19.

(ii) Determine the B_0 field with the ESR according to Step 52 and Eq. 6. Calculate the nuclear spin resonance frequency by multiplying the B_0 field strength in gauss by the gyromagnetic ratio in megahertz per gauss (Eq. 5). Calculate $\tau_0 = 1/(2f_L)$, to be set as the π-pulse spacing in the XY8-N sequence. Reasonable τ_0 values are between 300 and 2,000 ns.

(iii) Repeat the Rabi experiment (Step 56) to determine the $\pi/2$ and π-pulse durations. In some cases, the Rabi contrast decreases upon placing a sample on the surface because of background fluorescence of the sample or because the total internal reflection condition is no longer met. Note that the sample can also influence MW delivery.

(iv) Open correlSpecconfig.py in Notepad++. Set the π-pulse duration (`t_pi`), the XY8-N π-pulse spacing, τ_0 (`tau0`), and the MW frequency (`microwaveFrequency`), as determined in the previous steps. Choose the sampling of the swept delay, `t_corr`, so that at least 2 points per $1/f_L$ are recorded. The full duration of the sweep depends on the requirements of the measurement and can be kept short for initial nuclear spin detection

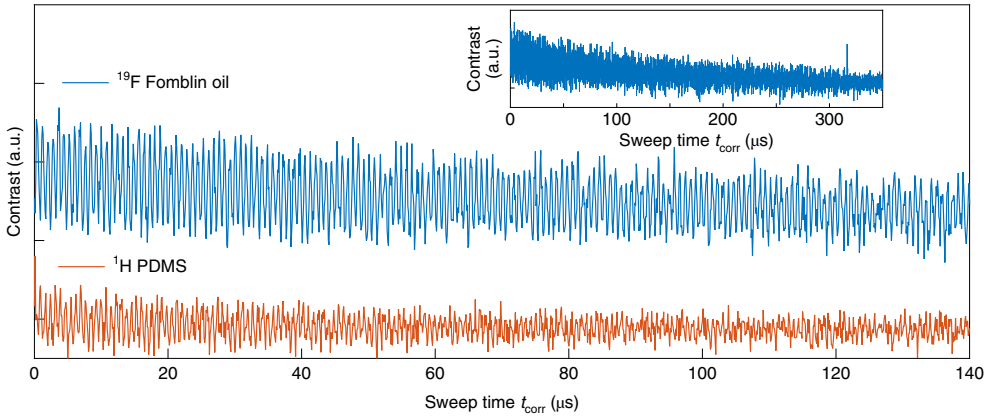

Fig. 19 | Correlation spectroscopy for NV-NMR sensing at 311 G. ^{19}F NMR detection in Fomblin oil (blue) and ^{1}H NMR detection in PDMS (orange). The oscillations are at the nuclear Larmor frequencies. Inset shows the full recorded data over 350 μs for the Fomblin oil. In both cases, 40-ns π pulses, an XY8-4 pulse sequence, 100-ns sampling intervals, and 10,000 samples were used. The ^{19}F data were averaged twice; the ^{1}H data were averaged ten times.

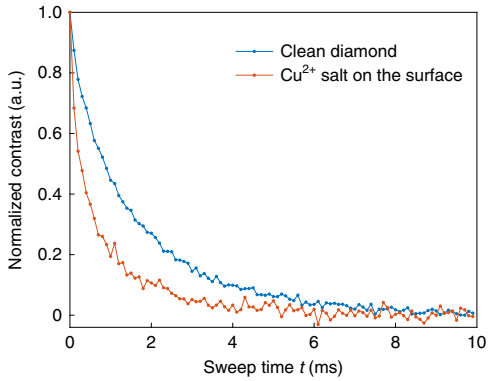

Fig. 20 | Electronic spin detection with NV-T1 relaxometry. NV-T1 decay of clean diamond (blue) compared to that with electronic spins (Cu^{2+}) on the diamond's surface (orange). Data are normalized to 1.0 at zero decay time. In both cases, the π-pulse duration is 36 ns and the number of samples is 1,000. The numbers of averages are 4 and 40 for the clean and Cu^{2+} cases, respectively. The Cu^{2+} data had to be averaged more times because of reduced contrast.

(e.g., $5/f_L$) or made long (several 10–100 μs) for recording the nuclear correlation time. Depending on the diamond, one should start by using $N = 1$ or 2. N should be optimized by comparing the SNR for the same total duration of the experiment. Use 10,000 samples and 2–4 averages (by setting the variables `Nsamples` and `Navg`, respectively). Set `t_readoutDelay` as determined in Step 53.

(v) Run `python mainControl.py correlSpecconfig`. The acquired data should show oscillation at f_L and look similar to those in Fig. 19.

? TROUBLESHOOTING

(C) **Running NV-T1 experiments for surface electronic spin detection ● Timing 4 h**

(i) Determine the NV-T1 relaxation time of the clean diamond according to Step 58 first (it should be around a few milliseconds).

(ii) Pipette a droplet of the sample on the diamond's surface at the laser spot. Keep in mind that the refractive index of the sample might change the total internal reflection condition, which in turn may lead to reduced sensitivity. When performing this step for the first time, we recommend using 1 M Cu^{2+}, Gd^{3+}, or Mn^{2+} solutions.

(iii) Repeat the Rabi experiment (Step 56) to determine the π-pulse duration. In some cases, the Rabi contrast decreases upon placing a sample on the surface because of background fluorescence of the sample or because the total internal reflection condition is no longer met. Note that the sample can also influence MW delivery.

(iv) Run `python mainControl.py T1config`. The acquired data should show a decreased NV-T1, as shown in Fig. 20.

Troubleshooting

Troubleshooting advice can be found in Table 2.

Table 2 | Troubleshooting table

Step	Problem	Possible reason	Solution
45	Cannot see a red spot on diamond	Laser light power is too low	Turn up the laser power; use laser goggles to protect your eyes Try to focus the laser spot more tightly
	Can only see a red stripe because of NV PL on diamond	Laser focus is not at the NV layer	Move the focusing lens to adjust the position of the focus
50	No ESR signal at zero field	Pulse sequence is not running	Check the pulse sequence on the oscilloscope and check whether all channels are active
		MW power is too low	Increase MW power (be careful not to exceed the maximum input of the amplifier) Move the laser spot closer to the MW wire Increase the full pulse sequence duration
51	Fewer than eight lines are observable in the ESR experiment	Not all transitions have the same amplitude and some might be weak	Relative resonance intensities can be changed by turning the laser light polarization with the $\lambda/2$ wave plate Increase MW power (be careful; do not exceed the maximum input of the amplifier)
		Lines are overlapping	Change the magnetic field direction slightly while observing the resonance positions
		Magnetic field strength is too strong	Check if the field is too strong and the resonance is out of the accessible frequency range. Move the magnets apart to reduce the field strength and record a spectrum at very low field
	Cannot see the hyperfine splitting in the ESR experiment	MW power is too high	Reduce the MW power and increase number of samples or averages
		Stray B_0 field gradient	Center the NVs in the laser spot between the magnets Use bigger magnets (>2-cm diameter) and increase distance between the magnets
		Intrinsic ESR linewidth is too broad	In very-high-density NV layers, the intrinsic ESR linewidth might be broader than the hyperfine splitting. Change NV implant parameters. Note that observation of the hyperfine splitting is not critical to the quantum sensing protocol
54	Cannot see a Rabi oscillation	Rabi frequency is very low	Extend the MW pulse duration to >1 μs and/or increase MW power (be careful not to exceed the maximum input of the amplifier) Check whether you set the MW frequency to the resonance of the NV measured in an ESR experiment
55	Poor Rabi contrast after optimization of laser polarization and optical repolarization	Background light/ fluorescence	Shield the experiment from room light
		Scattered laser light	Clean light guide and diamond surface Optimize the laser spot position on the diamond
56	Rabi frequency is very low	MW power is low	Increase MW power (be careful not to exceed the maximum input of the amplifier)
57	Cannot see a T2 relaxation decay, even though Rabi experiment works	IQ phase control is off	Turn on IQ phase control
	Cannot see RF loop signal in the XY8-*N* dynamic decoupling sequence	Signal is too weak	Reduce distance between RF loop and diamond Orient loop so that its *B* field is aligned along B_0 Use more windings Use an RF amplifier to increase the signal strength
59A(v) and 59B (v)	Cannot see a nuclear spin signal in XY8-*N* decay or correlation spectroscopy	SNR is not high enough	Increase number of averages Change *N* of the XY8-*N* sequence (higher *N* results in bigger signals, but contrast decreases with *N*; must find the optimum *N* for the experiment) Try to see a synthetic signal from an RF loop (Box 5). This lends a sense of the sensitivity and functionality of the experiment
		Sample is not in contact with the diamond	Clean the diamond and replace the sample. Often surface films and contaminants obfuscate the signal

Timing

The timing given below strongly depends on the user's experience. Most steps will be much faster after setting up the procedures and can take longer if performed for the first time.

Fabrication of NV diamond chips

Steps 1–11, acid cleaning: 2 h

Steps 12–17, annealing: 1 d

Construction of the quantum diamond spectrometer

Steps 18–25, experimental-control software installation: 1 d

Steps 26–32, PB and DAQ unit setup: 1 d

Steps 33–36, mounting and alignment of the AOM: 1 week

Steps 37–39, mounting magnets on an *xy*-translation stage with a rotating platform: 2 d

Steps 40–46, assembly of the excitation and detection components: 2 d

Step 47, construction of loop for MW delivery: 1 h

Steps 48 and 49, setup of signal source: 1 d

NV diamond characterization experiments

Step 50, finding the NV-ESR transition at ambient magnetic field: 2 d

Step 51, running NV-ESR—alignment and adjusting magnetic field: 2 d

Step 52, running NV-ESR—determining ESR resonance frequency and B_0 field strength: 2 h

Step 53, setting the timing between the readout pulses: 2 h

Steps 54 and 55, optimizing Rabi contrast: 1 d

Step 56, running Rabi—determining the π and $\pi/2$-pulse durations: 1 h

Step 57, running an NV Hahn-echo experiment—determine NV-T2 relaxation time: 1 h

Step 58, running an NV-T1 experiment—determine NV-T1 relaxation time: 2 h

Quantum sensing procedure for the detection of nuclear and electronic spins

Step 59A, running an XY8-*N* dynamic decoupling sequence for surface NMR signal detection: 2 h

Step 59B, running correlation spectroscopy for surface NMR signal detection: 2 h

Step 59C, running NV-T1 experiments for surface electronic spin detection: 4 h

Anticipated results

To illustrate the capabilities of the quantum diamond spectrometer, we here describe some results of nuclear and electronic spin sensing experiments. In all cases, we worked at a magnetic field of 311 G.

NV-NMR sensing with an XY8-*N* dynamic decoupling sequence

In Fig. 18, we show the NV-NMR detection of ^{1}H in PDMS and ^{19}F in Fomblin oil with an XY8-12 decay. At 311 G, the proton and the fluorine Larmor frequencies are 1.324 and 1.246 MHz, respectively. The magnetic noise at these frequencies causes dips in the XY8-12 decay at 378 ns and 401 ns. Experimental details can be found in the figure caption. Typically, the NV-T2 decay envelop is subtracted and the time axis is converted to a frequency axis with Eq. 3 (see inset, Fig. 18a).

NV-NMR sensing with correlation spectroscopy

In Fig. 19, we show the NV-NMR detection of ^{1}H in PDMS base and ^{19}F in Fomblin oil with correlation spectroscopy. Experimental details can be found in the figure caption. At 311 G, the proton and the fluorine Larmor frequencies are 1.324 and 1.246 MHz, respectively, both of which can be directly seen in the oscillation of the correlation data. Taking the Fourier transform of these data confirms the resonance frequencies (Fig. 21). The NMR signal can be identified unambiguously by changing the magnetic field strength, which causes frequency shifts in proportion to the gyromagnetic ratio. The oscillating correlation signal decays over time, largely because of spin decoherence or physical diffusion of the sample[30]. Sample diffusion leads to severe line broadening as compared to experiments that detect thermal nuclear spin polarization from larger volumes. Despite the line broadening, detection of sample diffusion indicates the ability to monitor dynamical molecular processes.

Electronic spin sensing with NV-T1 relaxometry

In Fig. 20, the NV-T1 relaxation of a bare diamond surface and that corresponding to a surface supporting a 1-M Cu^{2+} solution are compared. Experimental details can be found in the figure caption. The electronic noise of the unpaired spins in the Cu^{2+} ion reduces the NV-T1 relaxation

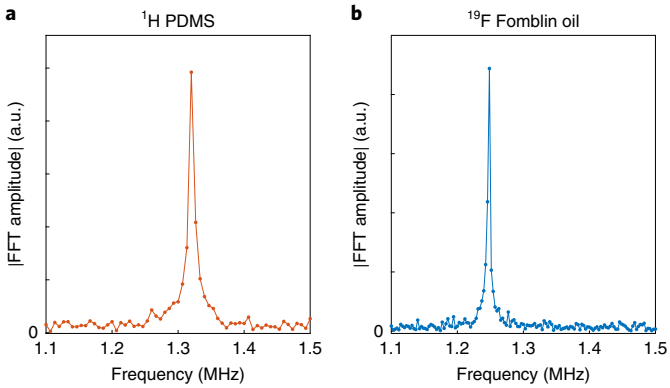

Fig. 21 | Fourier transform of the NV-NMR correlation signal at 311 G. Fourier transform data of time series displayed in Fig. 19. **a**, ^{1}H in PDMS. **b**, ^{19}F in Fomblin oil. Note that the sampling rate is different in the two cases. FFT, fast Fourier transform.

time significantly. The relaxation in both cases deviates from a pure mono-exponential decay, indicating an inhomogeneous NV ensemble, e.g., due to an NV depth distribution.

Reporting Summary

Further information on research design is available in the Nature Research Reporting Summary linked to this article.

Data availability

The primary data of this study are available from the corresponding authors upon reasonable request.

Code availability

The qdSpectro package is available to download from https://gitlab.com/dplaudecraik/qdSpectro and is licensed under the MIT License. The most recent version at the time of writing is v.1.0.1, but the user is encouraged to download the latest version and refer to the readme file for any patches and updates. The package is registered at https://doi.org/10.5281/zenodo.1478113, which points to the latest version.

References

1. Rule, G. S. and Hitchens, K. T. *Fundamentals of Protein NMR Spectroscopy*. (Springer, 2006).
2. Schweiger, A. and Jeschke, G. *Principles of Pulse Electron Paramagnetic Resonance*. (Oxford University Press, 2001).
3. Zalesskiy, S. S., Danieli, E., Blümich, B. & Ananikov, V. P. Miniaturization of NMR systems: desktop spectrometers, microcoil spectroscopy, and "NMR on a Chip" for chemistry, biochemistry, and industry. *Chem. Rev.* **114**, 5641–5694 (2014).
4. Fratila, R. M. & Velders, A. H. Small-volume nuclear magnetic resonance spectroscopy. *Annu. Rev. Anal. Chem.* **4**, 227–249 (2011).
5. Ardenkjaer-Larsen, J.-H. et al. Facing and overcoming sensitivity challenges in biomolecular NMR spectroscopy. *Angew. Chem. Int. Ed.* **54**, 9162–9185 (2015).
6. Staudacher, T. et al. Nuclear magnetic resonance spectroscopy on a (5-Nanometer)3 sample volume. *Science* **339**, 561–563 (2013).
7. Mamin, H. J. et al. Nanoscale nuclear magnetic resonance with a nitrogen-vacancy spin sensor. *Science* **339**, 557–560 (2013).
8. Lovchinsky, I. et al. Nuclear magnetic resonance detection and spectroscopy of single proteins using quantum logic. *Science* **351**, 836–841 (2016).
9. Shi, F. et al. Single-protein spin resonance spectroscopy under ambient conditions. *Science* **347**, 1135–1138 (2015).
10. Sushkov, A. O. et al. Magnetic resonance detection of individual proton spins using quantum reporters. *Phys. Rev. Lett.* **113**, 197601 (2014).
11. Lovchinsky, I. et al. Magnetic resonance spectroscopy of an atomically thin material using a single-spin qubit. *Science* **355**, 503–507 (2017).
12. Aharonovich, I. et al. Diamond-based single-photon emitters. *Rep. Prog. Phys.* **74**, 076501 (2011).

13. Schirhagl, R., Chang, K., Loretz, M. & Degen, C. L. Nitrogen-vacancy centers in diamond: nanoscale sensors for physics and biology. *Annu. Rev. Phys. Chem.* **65**, 83–105 (2014).
14. Doherty, M. W. et al. The nitrogen-vacancy colour centre in diamond. *Phys. Rep.* **528**, 1–45 (2013).
15. Rondin, L. et al. Magnetometry with nitrogen-vacancy defects in diamond. *Rep. Prog. Phys.* **77**, 056503 (2014).
16. Jelezko, F. & Wrachtrup, J. Single defect centres in diamond: a review. *Phys. Status Solidi A* **203**, 3207–3225 (2006).
17. Doherty, M. W. et al. Theory of the ground-state spin of the NV- center in diamond. *Phys. Rev. B* **85**, 205203 (2012).
18. Hincks, I., Granade, C. & Cory, D. G. Statistical inference with quantum measurements: methodologies for nitrogen vacancy centers in diamond. *New J. Phys.* **20**, 013022 (2018).
19. Meriles, C. A. et al. Imaging mesoscopic nuclear spin noise with a diamond magnetometer. *J. Chem. Phys.* **133**, 124105 (2010).
20. DeVience, S. J. et al. Nanoscale NMR spectroscopy and imaging of multiple nuclear species. *Nat. Nanotechnol.* **10**, 129–134 (2015).
21. Pham, L. M. et al. NMR technique for determining the depth of shallow nitrogen-vacancy centers in diamond. *Phys. Rev. B* **93**, 045425 (2016).
22. Herzog, B. E., Cadeddu, D., Xue, F., Peddibhotla, P. & Poggio, M. Boundary between the thermal and statistical polarization regimes in a nuclear spin ensemble. *Appl. Phys. Lett.* **105**, 043112 (2014).
23. Degen, C. L., Reinhard, F. & Cappellaro, P. Quantum sensing. *Rev. Mod. Phys.* **89**, 035002 (2017).
24. Abe, E. & Sasaki, K. Tutorial: magnetic resonance with nitrogen-vacancy centers in diamond—microwave engineering, materials science, and magnetometry. *J. Appl. Phys.* **123**, 161101 (2018).
25. Gullion, T., Baker, D. B. & Conradi, M. S. New, compensated Carr-Purcell sequences. *J. Magn. Reson.* **89**, 479–484 (1990).
26. Ryan, C. A., Hodges, J. S. & Cory, D. G. Robust decoupling techniques to extend quantum coherence in diamond. *Phys. Rev. Lett.* **105**, 200402 (2010).
27. Loretz, M. et al. Spurious harmonic response of multipulse quantum sensing sequences. *Phys. Rev. X* **5**, 021009 (2015).
28. Laraoui, A. et al. High-resolution correlation spectroscopy of ^{13}C spins near a nitrogen-vacancy centre in diamond. *Nat. Commun.* **4**, 1651 (2013).
29. Kong, X., Stark, A., Du, J., McGuinness, L. P. & Jelezko, F. Towards chemical structure resolution with nanoscale nuclear magnetic resonance spectroscopy. *Phys. Rev. Appl.* **4**, 024004 (2015).
30. Staudacher, T. et al. Probing molecular dynamics at the nanoscale via an individual paramagnetic centre. *Nat. Commun.* **6**, 8527 (2015).
31. Kehayias, P. et al. Solution nuclear magnetic resonance spectroscopy on a nanostructured diamond chip. *Nat. Commun.* **8**, 188 (2017).
32. Aslam, N. et al. Nanoscale nuclear magnetic resonance with chemical resolution. *Science* **357**, 67–71 (2017).
33. Glenn, D. R. et al. High-resolution magnetic resonance spectroscopy using a solid-state spin sensor. *Nature* **555**, 351–354 (2018).
34. Bucher, D. B., Glenn, D. R., Park, H., Lukin, M. D. & Walsworth, R. L. Hyperpolarization-enhanced NMR spectroscopy with femtomole sensitivity using quantum defects in diamond. Preprint at https://arxiv.org/abs/1810.02408 (2018).
35. Steinert, S. et al. Magnetic spin imaging under ambient conditions with sub-cellular resolution. *Nat. Commun.* **4**, 1607 (2013).
36. Sushkov, A. O. et al. All-optical sensing of a single-molecule electron spin. *Nano Lett.* **14**, 6443–6448 (2014).
37. Simpson, D. A. et al. Electron paramagnetic resonance microscopy using spins in diamond under ambient conditions. *Nat. Commun.* **8**, 458 (2017).
38. Ermakova, A. et al. Detection of a few metallo-protein molecules using color centers in nanodiamonds. *Nano Lett.* **13**, 3305–3309 (2013).
39. Schlipf, L. et al. A molecular quantum spin network controlled by a single qubit. *Sci. Adv.* **3**, e1701116 (2017).
40. Tetienne, J.-P. et al. Spin properties of dense near-surface ensembles of nitrogen-vacancy centers in diamond. *Phys. Rev. B* **97**, 085402 (2018).
41. Myers, B. A. et al. Probing surface noise with depth-calibrated spins in diamond. *Phys. Rev. Lett.* **113**, 027602 (2014).
42. Ofori-Okai, B. K. et al. Spin properties of very shallow nitrogen vacancy defects in diamond. *Phys. Rev. B* **86**, 081406 (2012).
43. Romach, Y. et al. Spectroscopy of surface-induced noise using shallow spins in diamond. *Phys. Rev. Lett.* **114**, 017601 (2015).
44. Ziegler, J. F., Ziegler, M. D. & Biersack, J. P. SRIM - the stopping and range of ions in matter (2010). *Nucl. Instrum. Methods Phys. Res. B* **268**, 1818–1823 (2010).
45. Lehtinen, O. et al. Molecular dynamics simulations of shallow nitrogen and silicon implantation into diamond. *Phys. Rev. B* **93**, 035202 (2016).
46. Yamamoto, T. et al. Extending spin coherence times of diamond qubits by high-temperature annealing. *Phys. Rev. B* **88**, 075206 (2013).
47. Haque, A. & Sumaiya, S. An overview on the formation and processing of nitrogen-vacancy photonic centers in diamond by ion implantation. *J. Manuf. Mater. Process.* **1**, 6 (2017).

48. Pezzagna, S., Naydenov, B., Jelezko, F., Wrachtrup, J. & Meijer, J. Creation efficiency of nitrogen-vacancy centres in diamond. *New J. Phys.* **12**, 065017 (2010).
49. Kim, M. et al. Decoherence of near-surface nitrogen-vacancy centers due to electric field noise. *Phys. Rev. Lett.* **115**, 087602 (2015).
50. Fávaro de Oliveira, F. et al. Tailoring spin defects in diamond by lattice charging. *Nat. Commun.* **8**, 15409 (2017).
51. Rosskopf, T. et al. Investigation of surface magnetic noise by shallow spins in diamond. *Phys. Rev. Lett.* **112**, 147602 (2014).
52. Sangtawesin, S. *et al*. Origins of diamond surface noise probed by correlating single spin measurements with surface spectroscopy. Preprint at https://arxiv.org/abs/1811.00144 (2018).
53. Atikian, H. A. et al. Superconducting nanowire single photon detector on diamond. *Appl. Phys. Lett.* **104**, 122602 (2014).
54. Tisler, J. et al. Fluorescence and spin properties of defects in single digit nanodiamonds. *ACS Nano* **3**, 1959–1965 (2009).
55. Pham, L. M. et al. Enhanced solid-state multispin metrology using dynamical decoupling. *Phys. Rev. B* **86**, 045214 (2012).
56. Aude Craik, D. P. L. *qdSpectro*. Zenodo. https://doi.org/10.5281/zenodo.1478113. (2019).
57. Fischer, R., Jarmola, A., Kehayias, P. & Budker, D. Optical polarization of nuclear ensembles in diamond. *Phys. Rev. B* **87**, 125207 (2013).
58. Jacques, V. et al. Dynamic polarization of single nuclear spins by optical pumping of nitrogen-vacancy color centers in diamond at room temperature. *Phys. Rev. Lett.* **102**, 057403 (2009).

Acknowledgements

This article is based on work supported by, or supported in part by, the US Army Research Laboratory and the US Army Research Office under contract/grant no. W911NF1510548. D.B.B. was partially supported by the German Research Foundation (BU 3257/1-1). D.P.L.A.C. was partially supported by the NSF STC 'Center for Integrated Quantum Materials' under cooperative agreement no. DMR-1231319.

Author contributions

D.B.B. led the development of the protocol, buildup of the quantum diamond spectrometer, and acquisition and analysis of data, informed by extensive past work in the Walsworth group and aided closely by D.P.L.A.C. and M.P.B. D.P.L.A.C. wrote the qdSpectro software package. M.J.T. prepared the NV-diamond chip and provided technical assistance in buildup of the quantum diamond spectrometer. O.B.D. performed a pilot run of the protocol and provided feedback to improve procedures. D.R.G. provided technical guidance to all aspects of the effort. R.L.W. supervised the project. All authors discussed the results and participated in writing the manuscript.

Competing interests

The authors declare no competing interests.

Additional information

Supplementary information is available for this paper at https://doi.org/10.1038/s41596-019-0201-3.

Reprints and permissions information is available at www.nature.com/reprints.

Correspondence and requests for materials should be addressed to D.B.B. or R.L.W.

Publisher's note: Springer Nature remains neutral with regard to jurisdictional claims in published maps and institutional affiliations.

Received: 30 August 2018; Accepted: 23 May 2019;
Published online: 26 August 2019

Related links

Key references using this protocol
DeVience, S. J. et al. *Nat. Nanotechnol.* **10**, 129–134 (2015): https://www.nature.com/articles/nnano.2014.313
Kehayias, P. et al. *Nat. Commun.* **8**, 188 (2017): https://www.nature.com/articles/s41467-017-00266-4
Steinert, S. et al. *Nat. Commun.* **4**, 1607 (2013): https://www.nature.com/articles/ncomms2588
Staudacher, T. et al. *Science* **339**, 561–563 (2013): https://science.sciencemag.org/content/339/6119/561

nature research

Corresponding author(s): Ronald Walsworth, Dominik Bucher

Last updated by author(s): Feb 7, 2019

Reporting Summary

Nature Research wishes to improve the reproducibility of the work that we publish. This form provides structure for consistency and transparency in reporting. For further information on Nature Research policies, see Authors & Referees and the Editorial Policy Checklist.

Statistics

For all statistical analyses, confirm that the following items are present in the figure legend, table legend, main text, or Methods section.

n/a	Confirmed	
☐	☒	The exact sample size (*n*) for each experimental group/condition, given as a discrete number and unit of measurement
☐	☒	A statement on whether measurements were taken from distinct samples or whether the same sample was measured repeatedly
☒	☐	The statistical test(s) used AND whether they are one- or two-sided *Only common tests should be described solely by name; describe more complex techniques in the Methods section.*
☒	☐	A description of all covariates tested
☒	☐	A description of any assumptions or corrections, such as tests of normality and adjustment for multiple comparisons
☒	☐	A full description of the statistical parameters including central tendency (e.g. means) or other basic estimates (e.g. regression coefficient) AND variation (e.g. standard deviation) or associated estimates of uncertainty (e.g. confidence intervals)
☒	☐	For null hypothesis testing, the test statistic (e.g. *F*, *t*, *r*) with confidence intervals, effect sizes, degrees of freedom and *P* value noted *Give P values as exact values whenever suitable.*
☒	☐	For Bayesian analysis, information on the choice of priors and Markov chain Monte Carlo settings
☒	☐	For hierarchical and complex designs, identification of the appropriate level for tests and full reporting of outcomes
☒	☐	Estimates of effect sizes (e.g. Cohen's *d*, Pearson's *r*), indicating how they were calculated

Our web collection on statistics for biologists contains articles on many of the points above.

Software and code

Policy information about availability of computer code

Data collection	Python, Matlab
Data analysis	Python, Matlab

For manuscripts utilizing custom algorithms or software that are central to the research but not yet described in published literature, software must be made available to editors/reviewers. We strongly encourage code deposition in a community repository (e.g. GitHub). See the Nature Research guidelines for submitting code & software for further information.

Data

Policy information about availability of data

All manuscripts must include a data availability statement. This statement should provide the following information, where applicable:

- Accession codes, unique identifiers, or web links for publicly available datasets
- A list of figures that have associated raw data
- A description of any restrictions on data availability

The data of this study are available from the corresponding authors upon reasonable request.

Field-specific reporting

Please select the one below that is the best fit for your research. If you are not sure, read the appropriate sections before making your selection.

☒ Life sciences ☐ Behavioural & social sciences ☐ Ecological, evolutionary & environmental sciences

For a reference copy of the document with all sections, see nature.com/documents/nr-reporting-summary-flat.pdf

Life sciences study design

All studies must disclose on these points even when the disclosure is negative.

Sample size	*Describe how sample size was determined, detailing any statistical methods used to predetermine sample size OR if no sample-size calculation was performed, describe how sample sizes were chosen and provide a rationale for why these sample sizes are sufficient.*
Data exclusions	*Describe any data exclusions. If no data were excluded from the analyses, state so OR if data were excluded, describe the exclusions and the rationale behind them, indicating whether exclusion criteria were pre-established.*
Replication	*Describe the measures taken to verify the reproducibility of the experimental findings. If all attempts at replication were successful, confirm this OR if there are any findings that were not replicated or cannot be reproduced, note this and describe why.*
Randomization	*Describe how samples/organisms/participants were allocated into experimental groups. If allocation was not random, describe how covariates were controlled OR if this is not relevant to your study, explain why.*
Blinding	*Describe whether the investigators were blinded to group allocation during data collection and/or analysis. If blinding was not possible, describe why OR explain why blinding was not relevant to your study.*

Reporting for specific materials, systems and methods

We require information from authors about some types of materials, experimental systems and methods used in many studies. Here, indicate whether each material, system or method listed is relevant to your study. If you are not sure if a list item applies to your research, read the appropriate section before selecting a response.

Materials & experimental systems

n/a	Involved in the study
☐	☐ Antibodies
☐	☐ Eukaryotic cell lines
☐	☐ Palaeontology
☐	☐ Animals and other organisms
☐	☐ Human research participants
☐	☐ Clinical data

Methods

n/a	Involved in the study
☐	☐ ChIP-seq
☐	☐ Flow cytometry
☐	☐ MRI-based neuroimaging

Antibodies

Antibodies used	*Describe all antibodies used in the study; as applicable, provide supplier name, catalog number, clone name, and lot number.*
Validation	*Describe the validation of each primary antibody for the species and application, noting any validation statements on the manufacturer's website, relevant citations, antibody profiles in online databases, or data provided in the manuscript.*

Eukaryotic cell lines

Policy information about cell lines

Cell line source(s)	*State the source of each cell line used.*
Authentication	*Describe the authentication procedures for each cell line used OR declare that none of the cell lines used were authenticated.*
Mycoplasma contamination	*Confirm that all cell lines tested negative for mycoplasma contamination OR describe the results of the testing for mycoplasma contamination OR declare that the cell lines were not tested for mycoplasma contamination.*
Commonly misidentified lines (See ICLAC register)	*Name any commonly misidentified cell lines used in the study and provide a rationale for their use.*

Palaeontology

Specimen provenance	*Provide provenance information for specimens and describe permits that were obtained for the work (including the name of the issuing authority, the date of issue, and any identifying information).*
Specimen deposition	*Indicate where the specimens have been deposited to permit free access by other researchers.*
Dating methods	*If new dates are provided, describe how they were obtained (e.g. collection, storage, sample pretreatment and measurement),*

Dating methods	*where they were obtained (i.e. lab name), the calibration program and the protocol for quality assurance OR state that no new dates are provided.*

☐ Tick this box to confirm that the raw and calibrated dates are available in the paper or in Supplementary Information.

Animals and other organisms

Policy information about studies involving animals; ARRIVE guidelines recommended for reporting animal research

Laboratory animals	*For laboratory animals, report species, strain, sex and age OR state that the study did not involve laboratory animals.*
Wild animals	*Provide details on animals observed in or captured in the field; report species, sex and age where possible. Describe how animals were caught and transported and what happened to captive animals after the study (if killed, explain why and describe method; if released, say where and when) OR state that the study did not involve wild animals.*
Field-collected samples	*For laboratory work with field-collected samples, describe all relevant parameters such as housing, maintenance, temperature, photoperiod and end-of-experiment protocol OR state that the study did not involve samples collected from the field.*
Ethics oversight	*Identify the organization(s) that approved or provided guidance on the study protocol, OR state that no ethical approval or guidance was required and explain why not.*

Note that full information on the approval of the study protocol must also be provided in the manuscript.

Human research participants

Policy information about studies involving human research participants

Population characteristics	*Describe the covariate-relevant population characteristics of the human research participants (e.g. age, gender, genotypic information, past and current diagnosis and treatment categories). If you filled out the behavioural & social sciences study design questions and have nothing to add here, write "See above."*
Recruitment	*Describe how participants were recruited. Outline any potential self-selection bias or other biases that may be present and how these are likely to impact results.*
Ethics oversight	*Identify the organization(s) that approved the study protocol.*

Note that full information on the approval of the study protocol must also be provided in the manuscript.

Clinical data

Policy information about clinical studies

All manuscripts should comply with the ICMJE guidelines for publication of clinical research and a completed CONSORT checklist must be included with all submissions.

Clinical trial registration	*Provide the trial registration number from ClinicalTrials.gov or an equivalent agency.*
Study protocol	*Note where the full trial protocol can be accessed OR if not available, explain why.*
Data collection	*Describe the settings and locales of data collection, noting the time periods of recruitment and data collection.*
Outcomes	*Describe how you pre-defined primary and secondary outcome measures and how you assessed these measures.*

ChIP-seq

Data deposition

☐ Confirm that both raw and final processed data have been deposited in a public database such as GEO.

☐ Confirm that you have deposited or provided access to graph files (e.g. BED files) for the called peaks.

Data access links *May remain private before publication.*	*For "Initial submission" or "Revised version" documents, provide reviewer access links. For your "Final submission" document, provide a link to the deposited data.*
Files in database submission	*Provide a list of all files available in the database submission.*
Genome browser session (e.g. UCSC)	*Provide a link to an anonymized genome browser session for "Initial submission" and "Revised version" documents only, to enable peer review. Write "no longer applicable" for "Final submission" documents.*

Methodology

Replicates	*Describe the experimental replicates, specifying number, type and replicate agreement.*

Sequencing depth	*Describe the sequencing depth for each experiment, providing the total number of reads, uniquely mapped reads, length of reads and whether they were paired- or single-end.*
Antibodies	*Describe the antibodies used for the ChIP-seq experiments; as applicable, provide supplier name, catalog number, clone name, and lot number.*
Peak calling parameters	*Specify the command line program and parameters used for read mapping and peak calling, including the ChIP, control and index files used.*
Data quality	*Describe the methods used to ensure data quality in full detail, including how many peaks are at FDR 5% and above 5-fold enrichment.*
Software	*Describe the software used to collect and analyze the ChIP-seq data. For custom code that has been deposited into a community repository, provide accession details.*

Flow Cytometry

Plots

Confirm that:

☐ The axis labels state the marker and fluorochrome used (e.g. CD4-FITC).

☐ The axis scales are clearly visible. Include numbers along axes only for bottom left plot of group (a 'group' is an analysis of identical markers).

☐ All plots are contour plots with outliers or pseudocolor plots.

☐ A numerical value for number of cells or percentage (with statistics) is provided.

Methodology

Sample preparation	*Describe the sample preparation, detailing the biological source of the cells and any tissue processing steps used.*
Instrument	*Identify the instrument used for data collection, specifying make and model number.*
Software	*Describe the software used to collect and analyze the flow cytometry data. For custom code that has been deposited into a community repository, provide accession details.*
Cell population abundance	*Describe the abundance of the relevant cell populations within post-sort fractions, providing details on the purity of the samples and how it was determined.*
Gating strategy	*Describe the gating strategy used for all relevant experiments, specifying the preliminary FSC/SSC gates of the starting cell population, indicating where boundaries between "positive" and "negative" staining cell populations are defined.*

☐ Tick this box to confirm that a figure exemplifying the gating strategy is provided in the Supplementary Information.

Magnetic resonance imaging

Experimental design

Design type	*Indicate task or resting state; event-related or block design.*
Design specifications	*Specify the number of blocks, trials or experimental units per session and/or subject, and specify the length of each trial or block (if trials are blocked) and interval between trials.*
Behavioral performance measures	*State number and/or type of variables recorded (e.g. correct button press, response time) and what statistics were used to establish that the subjects were performing the task as expected (e.g. mean, range, and/or standard deviation across subjects).*

Acquisition

Imaging type(s)	*Specify: functional, structural, diffusion, perfusion.*
Field strength	*Specify in Tesla*
Sequence & imaging parameters	*Specify the pulse sequence type (gradient echo, spin echo, etc.), imaging type (EPI, spiral, etc.), field of view, matrix size, slice thickness, orientation and TE/TR/flip angle.*
Area of acquisition	*State whether a whole brain scan was used OR define the area of acquisition, describing how the region was determined.*

Diffusion MRI ☐ Used ☐ Not used

Preprocessing

Preprocessing software

Provide detail on software version and revision number and on specific parameters (model/functions, brain extraction, segmentation, smoothing kernel size, etc.).

Normalization

If data were normalized/standardized, describe the approach(es): specify linear or non-linear and define image types used for transformation OR indicate that data were not normalized and explain rationale for lack of normalization.

Normalization template

Describe the template used for normalization/transformation, specifying subject space or group standardized space (e.g. original Talairach, MNI305, ICBM152) OR indicate that the data were not normalized.

Noise and artifact removal

Describe your procedure(s) for artifact and structured noise removal, specifying motion parameters, tissue signals and physiological signals (heart rate, respiration).

Volume censoring

Define your software and/or method and criteria for volume censoring, and state the extent of such censoring.

Statistical modeling & inference

Model type and settings

Specify type (mass univariate, multivariate, RSA, predictive, etc.) and describe essential details of the model at the first and second levels (e.g. fixed, random or mixed effects; drift or auto-correlation).

Effect(s) tested

Define precise effect in terms of the task or stimulus conditions instead of psychological concepts and indicate whether ANOVA or factorial designs were used.

Specify type of analysis: ☐ Whole brain ☐ ROI-based ☐ Both

Statistic type for inference
(See Eklund et al. 2016)

Specify voxel-wise or cluster-wise and report all relevant parameters for cluster-wise methods.

Correction

Describe the type of correction and how it is obtained for multiple comparisons (e.g. FWE, FDR, permutation or Monte Carlo).

Models & analysis

n/a	Involved in the study
☐	☐ Functional and/or effective connectivity
☐	☐ Graph analysis
☐	☐ Multivariate modeling or predictive analysis

Functional and/or effective connectivity

Report the measures of dependence used and the model details (e.g. Pearson correlation, partial correlation, mutual information).

Graph analysis

Report the dependent variable and connectivity measure, specifying weighted graph or binarized graph, subject- or group-level, and the global and/or node summaries used (e.g. clustering coefficient, efficiency, etc.).

Multivariate modeling and predictive analysis

Specify independent variables, features extraction and dimension reduction, model, training and evaluation metrics.